THEORETICAL AND EXPERIMENTAL ANALYSIS OF CRACK FORMATION IN REINFORCED CONCRETE

by

Kenneth Harold Murray

Thesis submitted to the Graduate Faculty of the
Virginia Polytechnic Institute
in partial fulfillment for the degree of

DOCTOR OF PHILOSOPHY

in

Civil Engineering

APPROVED:

Chairman: Dr. Richard M. Barker

Dr. George A. Gray

Dr. Raymond H. Myers

Dr. Henry M. Morris

Prof. Francis J. Maher

October, 1968

Blacksburg, Virginia

TABLE OF CONTENTS

ACKNOWLEDGMENTS

The author would like to express his appreciation to the members of his graduate committee for their guidance and assistance during his graduate studies, especially Dr. G. A. Gray who advised the author directly during the writing of this dissertation. Acknowledgment is also made of Dr. R. C. Heterick's assistance in the author's work with the computer.

Acknowledgment is made to NASA's Trainee Program which financed the author's graduate studies and other related expenses and to the Civil Engineering Department for financial aid in purchasing the necessary materials for this investigation.

Appreciation is also expressed to Messrs. K. G. McCauley and T. L. Poe for their technical help in the laboratory and to my fellow graduate students who took the time and energy to discuss and comment on this dissertation.

A most sincere acknowledgment of gratitude is expressed to Dr. Richard M. Barker for his many hours of preparation for classroom lectures and discussion which set the proper example for the prospective teachers in his class. For his suggestion of a topic worthy of investigation and his constant and close leadership and guidance of this dissertation, the author is very grateful. Because of these reasons and others, any new or different light shed on the subject of this dissertation, by the author, is only a reflection of this fine educator.

A special thanks is extended to my wife who edited and typed

this dissertation, who had faith in and encouraged the author along that rough road called graduate study.

LIST OF TABLES

LIST OF FIGURES

LIST OF FIGURES

I. INTRODUCTION

With the introduction and use of high strength materials, especially reinforcing steel, cracking and its control have become more important to the designer of modern reinforced concrete structures. Due to the properties inherent in concrete, cracks cannot be eliminated under normal working loads and, thus, the control of cracking becomes critical.

Large cracks are objectionable for a number of reasons, some of which are:

1. They may lead to corrosive attack of the reinforcement which may cause a strength reduction.
2. They may cause the structure to appear unstable or aesthetically unpleasant.
3. They may cause leakage in hydraulic structures.

Since cracking cannot be practically eliminated, it must be controlled. To control cracking, the problem of crack formation and development must be studied and understood completely. However, it is a complex problem involving a great many parameters and hence, conclusions regarding the significance of these parameters are difficult to obtain.

Crack development can be defined[1] in three stages according to the cause. In the first stage, primary cracks develop as a result of stresses caused by shrinkage, corrosive effects and low flexural loads in which the steel stress is well below 14 ksi. Since these cracks form first, they naturally will become the widest under increas-

ing load or age. In the second stage, secondary cracks develop due to the difference in extensibility between the concrete and steel, and also due to the bonding forces that exist between the two. A steel stress greater than 14 ksi exists in this stage of cracking. In the third stage, no further cracks form; therefore, this stage is referred to as the equilibrium stage. Since no further cracks form as the load is increased, the existing cracks widen. At this stage, the steel stress is usually greater than 30 ksi.

This dissertation considers the second stage of cracking and its influence on primary cracks. The width of the primary cracks depends on the last two stages. If no secondary cracks form, which means the primary cracks are at the minimum crack spacing, the primary crack width would be equal to the differences in elongation of the steel and concrete between cracks. But, since secondary cracks do form in almost all cases, the primary crack width will depend on the number of secondary cracks that form between primary cracks.

This dissertation uses as its experimental model, the axially reinforced concrete cylinder, in tension, to study the effect of bond distribution on crack width and spacing. This model has been used by many researchers, both in this country and in Europe. The analytical model is a finite element representation of the axially reinforced concrete cylinder in tension. The results of the analytical model are then evaluated to determine a prediction equation for crack width and spacing. These equations are compared with a large volume of data from beam tests recorded in the literature. A statistical analysis is also made of this large volume of data to determine the

important physical parameters. A prediction equation is also developed from a non-linear regression analysis of this data.

II. LITERATURE REVIEW

To review the literature before the introduction of deformed reinforcing bars seems quite useless and, therefore, only a few comments will be made concerning tests on smooth or plain bars. All investigations on cracking in which deformed bars are compared with smooth bars, it was found that the modern deformed bar was a much better crack size reducer than any other bar except a threaded bar. It is quite obvious that threaded bars have an economical disadvantage because of their high cost in comparison to the deformed bar. The literature has been reviewed with the basic assumption that deformed bars are the best bars for practical construction.

This chapter will be divided into two parts, theoretical and experimental. These sections will not be mutually exclusive, as the same study might well appear in both. The theoretical section will deal with the analytical representation of the cracking phenomena as it has been developed in the literature. The experimental section will review experimental data recorded in the literature. Major parameters and the range of study will be included, along with basic conclusions.

Theoretical

One of the first theoretical investigations was reported by Watstein and Parsons[2] in 1943. It dealt only with symmetrically reinforced concrete prisms subjected to axial tension. The basic assumptions for the development of their theory were:

1. The steel stress does not exceed the proportional limit,

2. The steel is uniform in size and shape, and continuous throughout the length of specimen,

3. The tensile stress in the concrete is uniformly distributed across the cross section, and

4. The strain in the concrete is proportional to the stress.

Even with these restrictions, Watstein and Parsons' theoretical evaluation of crack width and spacing is very important and, therefore, is reviewed in detail.

Using the model shown in Figure 1, which is a tensile section between cracks, the tensile stress in the concrete f_{tx} at a distance x from a crack, is equal to the force transmitted by bond divided by the concrete area, or

$$f_{tx} = \frac{N\pi D}{A_c} \int_0^x u_x dx = \frac{4p}{D} \int_0^x u_x dx \qquad (1)$$

where N = number of reinforcing bars*

D = diameter of reinforcement

A_c = concrete area

x = distance along specimen from primary crack

u_x = bond stress distribution

p = percentage of steel, $N\pi D^2/4A_c$.

Then the stress in the reinforcement f_{sx} at a distance x from a primary

---

* Notation is defined when first used and also in Appendix A

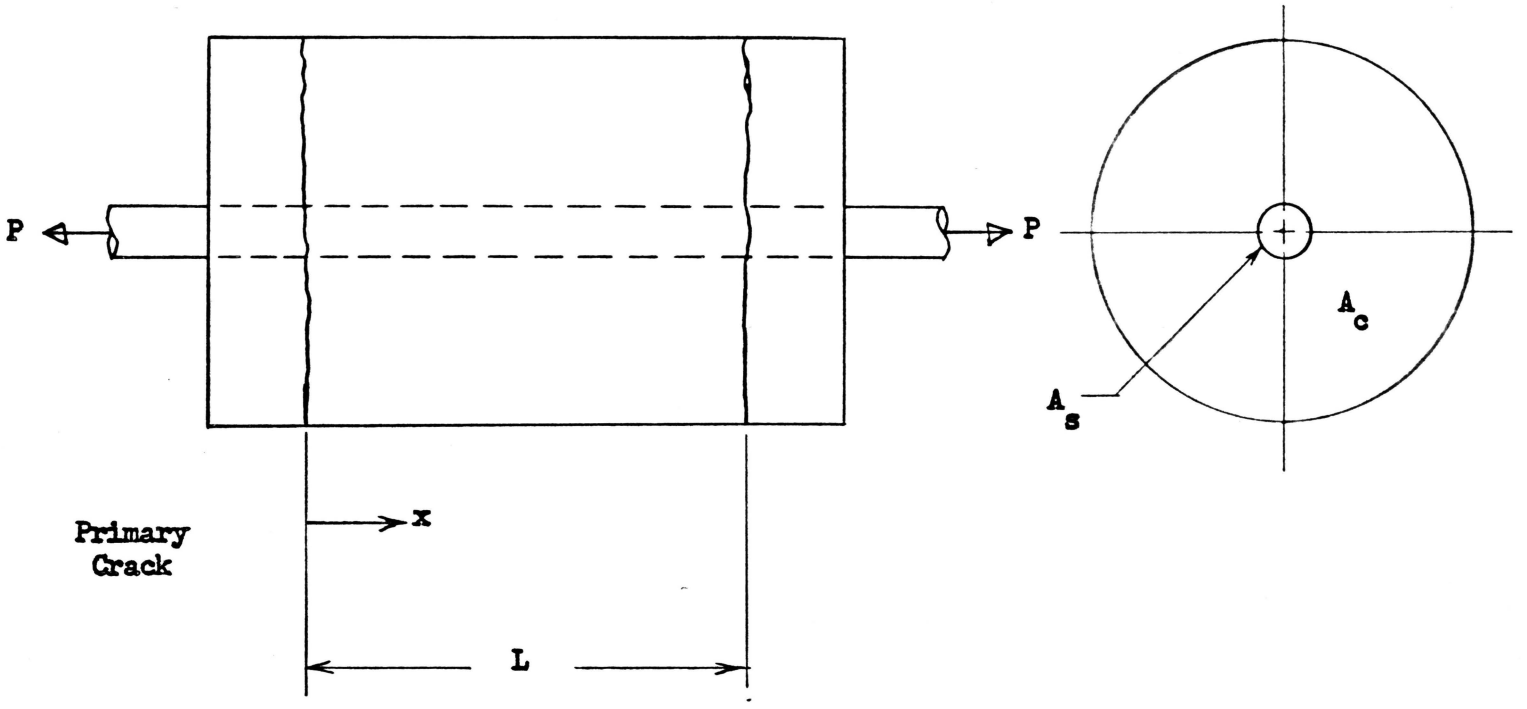

FIGURE 1. Axially Reinforced Concrete Model in Tension

crack is given by

$$f_{sx} = f_s - \frac{N\pi D}{A_s} \int_0^x u_x dx = f_s - \frac{4}{D} \int_0^x u_x dx \qquad (2)$$

where f_s = tensile stress in the reinforcement at a crack

A_s = area of reinforcement.

It can be shown from experimental investigations that the maximum concrete stress occurs between two existing cracks at the midway point along the longitudinal axis, or at L/2. If in Equation (1) x is set equal to L/2 and f_{tx} equal to the tensile capacity of the concrete f'_t, the equation becomes,

$$f'_t = \frac{4p}{D} \int_0^{L/2} u_x dx \qquad (3)$$

where L = maximum possible crack spacing.

Equation (3) is the defining equation for maximum crack spacing. Of course, the bond stress distribution must be defined before the spacing can be calculated. Quite obviously this is a basic problem which will be discussed in fuller detail later.

Watstein and Parsons make a variable transformation to simplify the equations. Using the fact that the bond stress distribution can be expressed as

$$u_x = u_m f(x/L) \qquad (4a)$$

where u_m = maximum bond stress

and also letting

$$Q = x/L \tag{4b}$$

Equation (3) becomes

$$f'_t = \frac{4p}{D} \int_0^{\frac{1}{2}} f(Q)\, dQ \tag{5}$$

This expression can be solved for L and the general solution is

$$L = \frac{C_1 f'_t D}{u_m p} \tag{6}$$

$$\text{where } C_1 = \frac{1}{4 \int_0^{\frac{1}{2}} f(Q)\, dQ} \tag{6a}$$

Watstein and Parsons continue their theoretical presentation by defining the slip per unit length as the difference between the strains in the steel and concrete or

$$s_x = \frac{f_{sx} - n f_{tx}}{E_s} \tag{7}$$

where s_x = slip per unit length

n = modular ratio E_s/E_c

E_s = modulus of elasticity for steel.

The crack width then can be determined by summing all of the unit slips from zero to L or, because of symmetry about L/2,

$$W = 2 \int_{o}^{L/2} s_x \, dx \tag{8}$$

where W = maximum crack width.

Combining all of the above equations gives the general solution for the maximum crack width due to axial loading,

$$W = \frac{C_1 f'_t}{u_m p E_s} \left[f_s - C_2 f'_t (1/p + n) \right] \tag{9}$$

$$\text{where } C_2 = 8C_1 \int_{o}^{\frac{1}{2}} dQ \int_{o}^{Q} f(Q) \, dQ \tag{9a}$$

If Equation (9) is set equal to zero, the following expression for f_s results

$$f_{so} = C_2 f'_t (1/p + n) \tag{10}$$

where f_{so} = theoretical value of steel stress at first cracking. At first glance, this seems to be the steel stress at which cracking first occurs, but this is only an extrapolated value. It does present a good way to evaluate C_2 experimentally. C_1 must also be evaluated by experimental methods, since no direct solution exists at present.

Watstein and Parsons made the following comments on their theoretical presentation:

1. Perhaps the largest errors are those in estimates of n, as the strains are not proportional to the stresses as was assumed.
2. Since shearing effects were not included, Equation 1

over-estimates the tensile resistance of the concrete.

3. Also by neglecting shearing deformations, the variation of tensile stress in the concrete is neglected. Actually the concrete stress is greatest next to the reinforcement, and diminishes as you move away from the reinforcement.

Reis and Boresi[3] presented experimental data which confirms Watstein and Parsons' third comment.

The next important contribution to the theory of crack formation was made by Hognestad[4] in 1962. He discusses the random nature of cracking and explains the concept of minimum and maximum spacing of cracks. The minimum spacing, L_m, is reached when a tensile force of sufficient magnitude to form an additional crack between two existing cracks can no longer be transmitted by bond from steel to concrete. The maximum spacing L then is equal to twice the minimum spacing or

$$L = 2L_m \tag{11}$$

Using the above information and an approach similar to Watstein and Parsons, Hognestad derives the following equation for maximum crack spacing

$$L = \frac{f'_t A_e D}{r_1 u_m 2A_s} \tag{12}$$

where A_e = effective concrete area in tension

r_1 = factor reflecting bond distribution

He also develops an equation for maximum crack width

$$W = \frac{D f_s}{p_e K_1} \tag{13}$$

where $p_e = A_s / A_e$ (13a)

$$K_1 = 2 r_1 u_m E_s / f'_t \tag{13b}$$

It should be noted that in Hognestad's development, the elongation of the concrete is neglected. Also, the quantity A_e is not defined precisely and, therefore, the accuracy depends a great deal on defining this effective concrete area.

Bresler and Bertero[5] presented a finite element approach to cracking in reinforced concrete. The idealized specimen consisted of steel, bond and concrete elements. Since the finite element programs presented by Wilson[6] handles combinations of materials, the idealization is accomplished by assigning the proper modulus of elasticity and Possion's ratio to each element type.

The steel and concrete elements are as usual, but the bond element had a reduced modulus of elasticity and an increased Possion's ratio ($E = 270$ ksi, $\nu = 0.495$). These values are approximately the same as for rubber. They report that only limited tests had been run, but the results seemed to compare quite favorably with their experimental data in certain areas.

Broms[7] presented a very interesting theory about the extent of flexural cracks using circles inscribed between cracks. Figure 2 shows

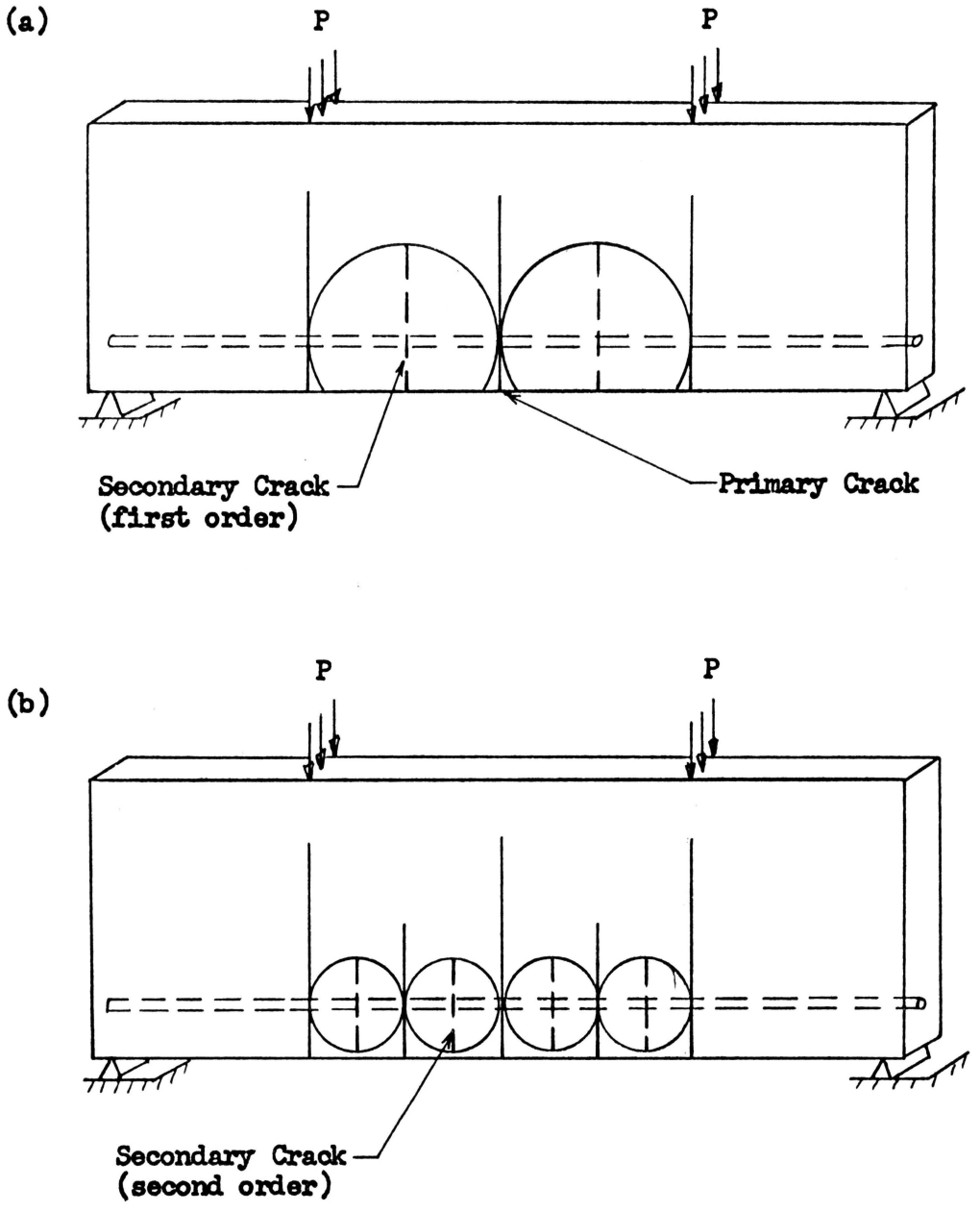

(From Reference 7)

FIGURE 2. Mechanism of Tension Cracking in Flexural Members

a typical beam with constant moment region and its crack pattern as indicated by Broms. He explains that on the circumference of each circle, the concrete stress is zero. Inside the circle, there are tensile stresses and outside compressive stresses exist in the concrete. The (b) part of Figure 2 corresponds to experimentally recorded compressive strains between cracks on the surface. The secondary cracks of second order do not reach the surface as indicated in Figure 2(b). He also indicates that this theory can be applied to axially reinforced tension members.

Ngo and Scordelis[8] presented another approach to the problem of cracking in reinforced concrete beams using finite elements. They developed a bond element shown in Figure 3 which consisted of linear springs in two directions. They use this element to calculate deflections in beams and found their results matched quite well with experimental data.

The biggest draw-back to Ngo and Scordelis' element is determining values for the stiffness of the springs. There is not much experimental data available to evaluate these stiffnesses, especially in the perpendicular direction. They used a range from 1.8 to 2.6 x 10^3 kips per inch for the stiffness parallel to the steel and "a very high number" for the stiffness perpendicular to the steel.

The most recent verification of the use of finite elements in reinforced concrete research was recorded by Nilson[9] in September, 1968. He developed an analytical model which permits the inclusion of (a) the influence of reinforcement, (b) changing topology due to progressive cracking, (c) realistic bond stress transfer between con-

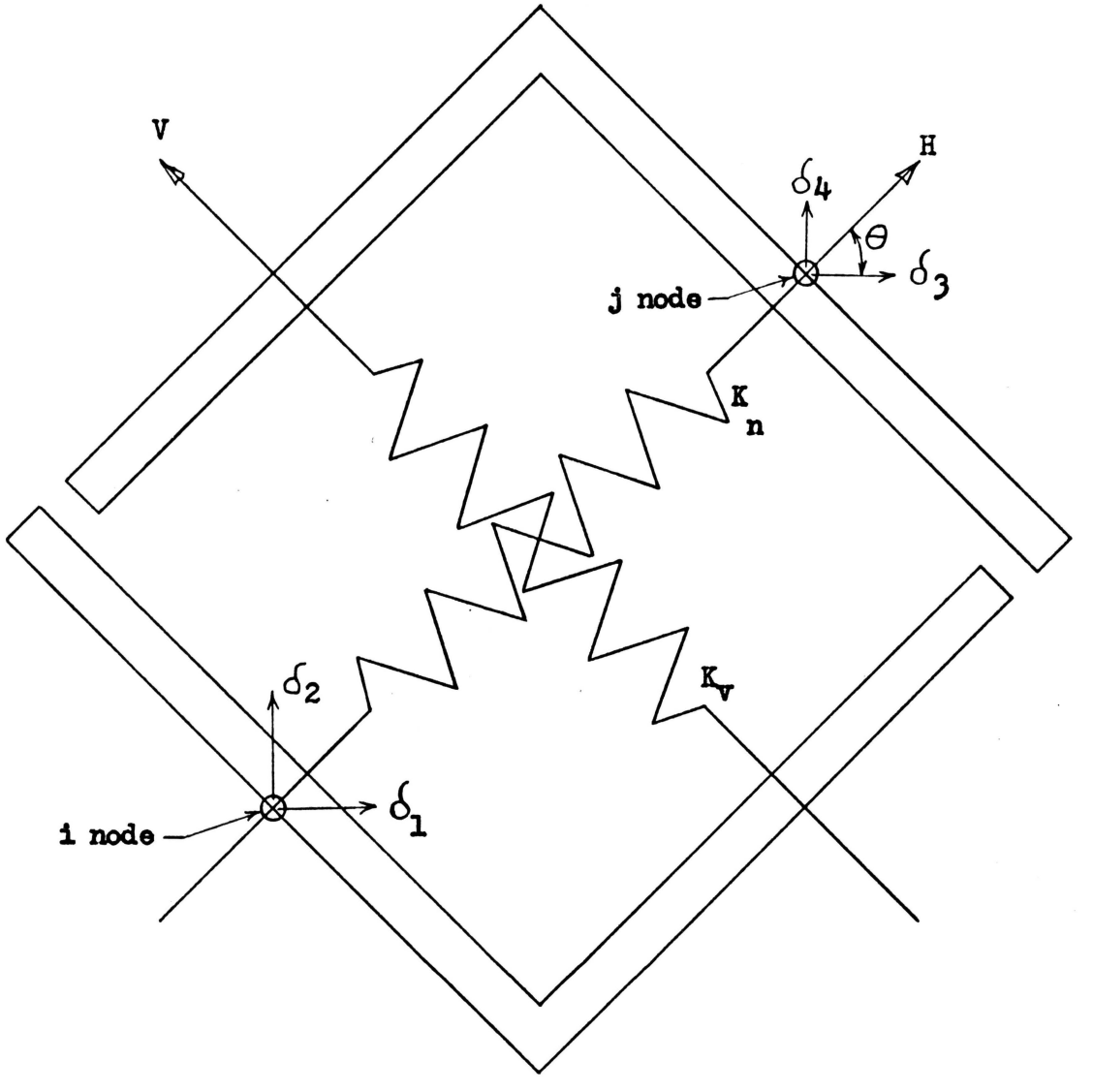

(From Reference 8)

FIGURE 3. Bond Linkage Element by Ngo and Scordelis

crete and reinforcement, and (d) nonlinear material properties. His bond element was the same as the one developed by Ngo and Scordelis[8]. Using this bond element, Nilson checked his analytical model against experimental results of Broms[7]. The comparison was quite favorable and Nilson concluded that his model was correct. One interesting point of information which was obtained, was the measuring of bond destruction. This length of bond destruction influences the concrete steel and bond stresses.

His concluding remark was: "A finite element analysis of reinforced concrete behavior provides a valuable supplement to laboratory investigations, and may lead to important changes in methods of design." This is an important concept which was emphasized in the development of this dissertation.

In 1966, Gergely and Lutz[10] presented a new approach to the analysis of crack formation. They took existing data and analyzed it statistically to obtain a prediction equation for maximum crack width. It was not a standard statistical analysis because they used other investigators' combinations of variables and tried to find some other combination which best fitted the large mass of data already recorded in the literature. This required that some combinations be transformed into log-equations so that a linear regression analysis could be performed. The transformed log-equation tends to smooth out the data and because of this will give questionable results when the range of the data is more than one log cycle. The following major conclusions were reached regarding the factors affecting the crack width:

1. The steel stress is the most important variable.
2. The cover thickness is an important variable, but is not the only consideration.
3. The bar diameter is not a major variable.
4. The bottom crack width increases with the strain gradient.
5. The major variables are the effective area of concrete, the number of bars, the side or bottom cover and the steel stress.

Experimental

Clark[11] in 1956 reported test results on 26 beams and 28 slabs. Crack width and spacing were recorded for each beam at seven different stress levels from 15 ksi to 45 ksi in 5 ksi steps. There were only two different total depths, 15 and 23 inches, both with a constant width of six inches. The beams had either one or two reinforcing bars which varied in size from number six to eleven. The concrete strength was relatively constant from beam to beam. The concrete cover varied because of bar sizes, but was relatively constant in each different height group.

Clark uses his data to evaluate Watstein and Parsons'[2] constants C_1 and C_2 and obtains C_1 as a function of cover/depth and C_2 as a pure constant. He then uses these constants to predict crack spacing and width, but found considerable scatter in the data. His qualitative conclusions are in agreement with most researchers, and they can be stated as follows:

1. Average crack width is proportional to the product of D/p and (h-d)/d, where D is bar diameter, p is steel percentage, h is total height and d is depth of the beam.
2. Average crack width is proportional to the increase of steel stress beyond that causing initial cracking.
3. Average crack spacing decreases rapidly with an increase in steel stress beyond that causing the first crack, and
4. Average crack spacing approaches a constant value at "high" steel stresses.

In 1958, Chi and Kirstein[12] presented test results on 16 beams at six different stress levels from 15 ksi to 40 ksi in 5 ksi increments. This resulted in 86 data points which could be used to evaluate analytical results. The major parameter studied in this investigation was concrete strength, which was varied from 2000 psi to 6000 psi.

Both crack width and spacing were recorded at each stress level, with the exception of a few cases where readings were not recorded. The width of cracks was measured using six-inch Tuckerman gages. The authors reported a complication which led to a great deal of discussion which will be reviewed later. The complication was due to the six-inch gage length of the Tuckerman gages. Since the minimum crack spacing was less than six inches in most beams, the gage actually covered more than one crack in some beams. This required the authors to exercise judgment in deciding which gage readings to use in determining average and maximum widths of cracks.

Chi and Kirstein summarize their work with the following:

1. The minimum average spacing of cracks was found to be proportional to the product of the diameter of the reinforcing bar and the ratio of the assumed effective area to the fully-developed area of concrete.
2. The average width of the cracks at the steel is given by the product of the average minimum spacing of the cracks and a function of the computed steel strain.
3. Concrete strength has practically no effect on the formation of cracks.

Bertero[13] and Borges[14] while discussing the article by Chi and Kirstein[12] comment on the problem of measuring crack widths with the Tuckerman gages. They both indicate that this method automatically neglects the tensile strain in the concrete. In the original article, the authors had justified this method of measuring crack width because the tensile strain in the concrete is quite small and even compressive strains may exist between cracks. The discussers also indicated that the actual measuring of the crack width was open to too much judgment and, therefore, was not good experimental procedure. But, in Chi and Kirstein's closure, they indicated that since maximum crack widths was the important measured quantity, the Tuckerman gage was good enough. In most cases, the crack of maximum width was set apart from all other cracks and, therefore, was usually alone inside the gage length.

Bertero[13] also takes issue with Chi and Kirstein[12] over the compressive strains they reported between cracks. The authors explained in their closure that perhaps this phenomenon can be explained in the

following way: After cracks become numerous and close to one another, the flexural stresses between successive cracks diminish, and the stresses are predominately due to shear between reinforcement and concrete. While this phenomenon is not yet fully understood, it is conceivable that the distortion due to shear can produce either compression or tension on the face of the beam. It must be understood that these are small strains.

In 1961, Hognestad[4] presented experimental data along with his theoretical developments, which have already been discussed. His experimental investigation studied the following parameters:

1. Bar diameter
2. Beam width
3. Beam depth
4. Concrete cover

The effect of these parameters on crack width and spacing was studied by testing 36 beams. Each of the above beams had crack width recordings at steel stress levels of 20, 30, 40 and 50 ksi, and crack spacing at a steel stress of 30 ksi.

Hognestad drew the following conclusions from his experimental investigation:

1. Maximum crack width is essentially proportional to steel stress.
2. Maximum crack width is essentially independent of concrete strength, beam width and beam depth.
3. Maximum crack width is strongly influenced by the thickness of concrete cover.

4. Maximum crack width is not directly proportional to crack spacing.

The fourth conclusion does not agree with Chi and Kirstein's[12] second conclusion presented earlier. It seems that Hognestad's is backed by a theoretical analysis by Rusch and Rehm[15].

In 1965, Broms[7] reported an investigation using 37 tension members and 10 flexural members in which crack width and spacing were recorded. Broms first tested very long tensile specimens to determine minimum spacing of cracks, then tested a small member with the minimum crack spacing as its length. In Part II of his article, he records crack spacing for 15 beams and 10 tensile specimens at steel stresses of approximately 30, 50 and 70 ksi.

Broms measured internal cracking in a few specimens by injecting a resin EPOCAST 530 into the specimen at the maximum load. The applied load was maintained while the specimen was coated with resin and allowed to dry. This sealed all exterior cracks and also one end of the preformed channel through which the resin was injected. The load was maintained while the resin was injected under pressure and hardened, thus preserving the total crack pattern. Later the specimen was cut open parallel to the reinforcement by means of a diamond saw. All cracks, maintained in their original shape by the hardened resin, were observed and examined by a hand microscope. A number of cracks were observed which never reached the exterior of the specimen.

Bresler and Bertero[5] reported an investigation of load history on cracking. They instrumented the reinforcing bars by splitting them and milling a groove for electrical strain gages. The bars were

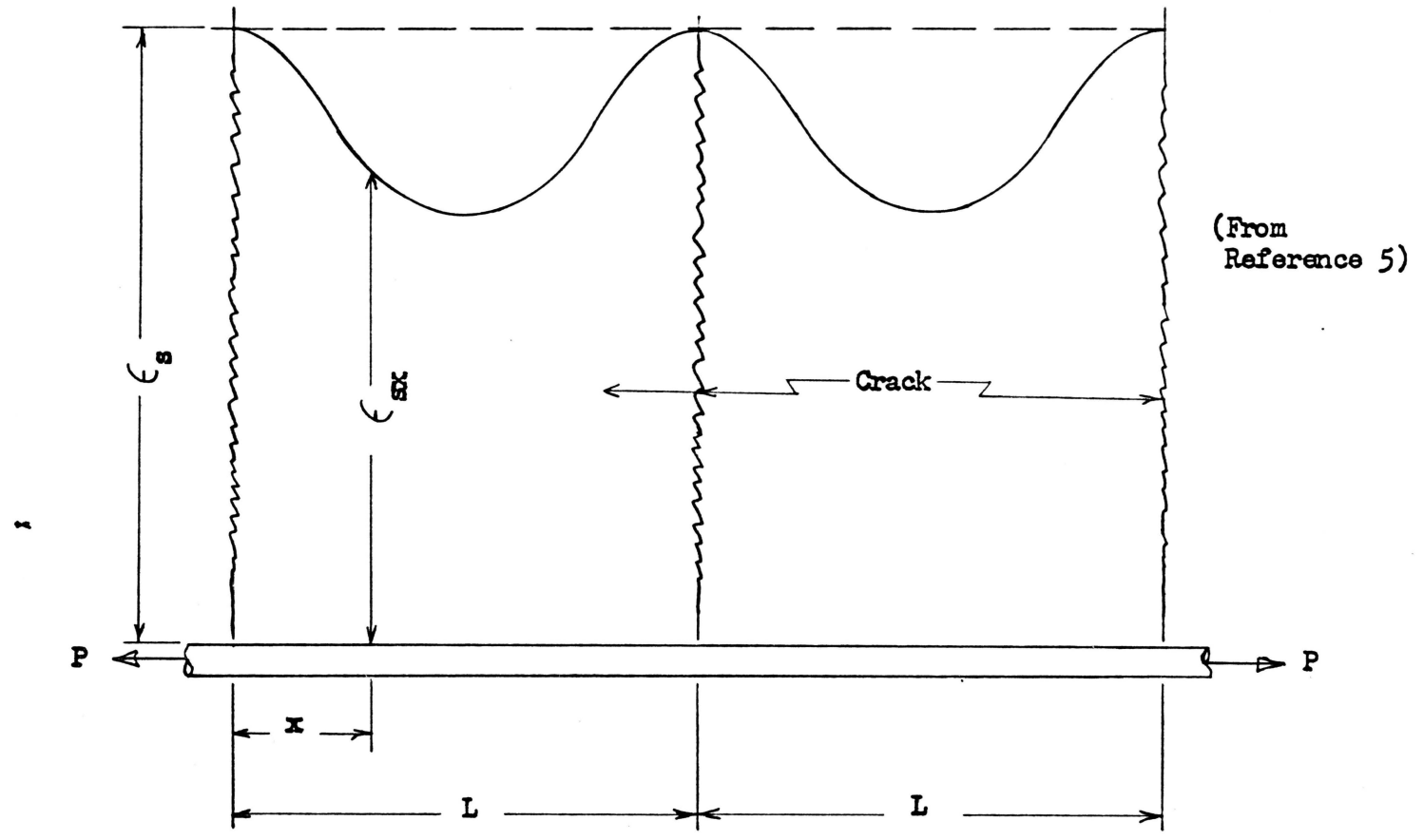

FIGURE 4. Steel Strain Distribution in Cracked Prism

welded together and cast in the specimens. When the specimens were tested, steel strain could be recorded all along the length of reinforcement. The typical shape of this distribution is shown in Figure 4.

They concluded from their tests that repeated loads caused decay of the bond between steel and concrete. This means that load history affects the crack width and spacing and, therefore, must be considered in design.

III. STATISTICAL APPROACH TO CRACK FORMATION

The idea of a statistical approach to cracking has been mentioned by a number of authors, but only Gergely and Lutz[10] have taken the idea and used it. With the large mass of data already recorded, it would seem quite informative to analyze it statistically. The basic objective of this chapter is to obtain information about the major parameters in crack formation and, if possible, to obtain an equation which will accurately predict crack width and spacing. The first part will be a general discussion of the statistical procedure used and the last part will describe how this procedure was used and the results.

The basic statistical approach was a non-linear regression analysis developed by R. C. Heterick[16]. Heterick used his algorithm to obtain design equations by using as data "good" designs obtained in the conventional way. He generated enough of this data to apply his algorithm and obtain very accurate design equations. As he notes, this algorithm can be used with experimental data.

In simple terms, the algorithm takes a set of data and proceeds to fit it into the form

$$Y = a_o + X_1^{a_1} \cdot X_2^{a_2} \cdot X_3^{a_3} \cdots X_n^{a_n} \qquad (14)$$

where Y is the dependent variable

X_i are the independent parameters

a_i are the determined coefficients for best fit.

The first step is to make a log transformation so that a step-wise linear regression analysis can be run.

To explain step-wise linear regression, the following example with only three parameters will be used.

$$Y - a_o = X_1^{a_1} X_2^{a_2} X_3^{a_3} \tag{15}$$

The log transformation becomes

$$\log (Y - a_o) = a_1 \log X_1 + a_2 \log X_2 + a_3 \log X_3 \tag{16}$$

For convenience, the log terms are written as b terms, so that,

$$Y' = a_1 b_1 + a_2 b_2 + a_3 b_3 \tag{17}$$

The algorithm begins with b_1, b_2 and b_3 and runs the regression on each independently and determines which one best represents Y'. For illustration, say b_2 is best. So now, the algorithm takes $b_2 + b_1$ and $b_2 + b_3$ and checks to see which of these is best. And again for illustration, assume $b_2 + b_3$ is best. The last step is to add b_1 or check $(b_2 + b_3) + b_1$ for its contribution to best fit; if it does not improve the fit, then b_1 is not a statistically important parameter. The final model would look like this

$$Y' = a_2 b_2 + a_3 b_3 \tag{18}$$

The algorithm then defines the constants from the last regression analysis.

The most important process begins now with the non-linear

regression analysis by iteration. Using the statistically important parameters and also the values of the constants from the first approximation, the regression analysis is performed.

The final results are an equation of the form of Equation (14) and an indicator of goodness of fit, the correlation coefficient, R. R is defined as:

$$R = \left[\frac{\sum_{i=1}^{n} Y_i^2 - \sum_{i=1}^{n} e_i^2}{\sum_{i=1}^{n} Y_i^2} \right]^{\frac{1}{2}} \qquad (19)$$

where Y_i = individual value of the dependent variable

e_i = error of approximation.

R is maximum, when the fit is very good, but always less than or equal to one. If equal to one, the calculated and actual values are identical.

Care must be taken in analyzing the results from this approach when experimental data is used. Important statistical parameters are not always important physical parameters. Knowledge of the data set is extremely important when drawing conclusions from this algorithm.

The data used in this algorithm were discussed in Section II but will again be listed. Clark[11] reported results on 26 beams at seven different stress levels giving a total of 182 points. This was reduced to 165 points because some readings were not recorded. Chi and Kirstein[12] presented test results on 16 beams at six different stress levels giving a total of 96 points. This was reduced to 87

because again some readings were not recorded. Hognestad[4] presented results on 36 beams at four different stress levels giving a total of 144 points. Seven beams were not included because they contained plain bars, leaving a total of 110 points of recorded data. Broms[7] reported on 15 beams at three stress levels or a total of 45 points, but again four points are not recorded leaving only 41 points. The grand total of data points was 403.

These 403 data points were statistically analyzed using Heterick's algorithm. From the results of this analysis some data points were removed. The basis for removal was that the point was three or more standard deviations away from the calculated value. In most cases, these "bad" points were at very low or very high loads. Other "bad" points were from a single beam at different load levels, indicating a possible "bad" beam. There were only 26 such points in all of the data, leaving a total of 378 points for the final statistical analysis.

The dependent variable in the algorithm was the maximum crack width and the independent parameters were:

1. Steel stress
2. Bar diameter
3. Total depth of beam
4. Width of beam
5. Cover
6. Concrete compressive strength, and
7. Number of bars.

None of the above were rejected as insignificant parameters with

the following algorithm constants:

1. Minimum F ratio of 1.0
2. Minimum correlation coefficient improvement of 0.0001, and
3. The leading constant held invariant at zero.

The correlation coefficient from the linear regression was 0.9992 which is quite good, but from the more exact non-linear regression, it was only 0.981. This points out the error in using the log transformed linear regression on any set of data. The 0.981 indicates that the fit is not perfect, but that it is a good fit. The following equation is the final result:

$$W = 0.000012\,(f_s)^{1.29}\,(h)^{-0.036}\,(D)^{0.183}\,(b)^{0.883}\,(COVER)^{0.738}\,(f'_c)^{0.037}\,(N)^{-0.182} \qquad (20)$$

where W = crack width (inches)

f_s = steel stress (ksi)

h = total depth of beam (inches)

b = width of beam (inches)

COVER = concrete cover (inches)

f'_c = concrete compressive strength (ksi)

N = number of bars

Heterick's algorithm was also used to obtain a prediction equation for crack spacing using the same independent parameters and constants. The correlation coefficient of this fit was 0.949. The

crack spacing was determined to be

$$L_a = 7.84\,(f_s)^{-0.560}\,(h)^{0.443}\,(N)^{-0.835}\,(D)^{-0.612}$$

$$(f'_c)^{-0.099}\,(b)^{0.488}\,(COVER)^{0.064}$$

where L_a = average crack spacing (inches)

the other parameters were defined above.

It should be noted that these equations only define crack width and spacing in a region of constant moment. Nearly all recorded data is on beams with constant moment section. No data points for concentrated or uniform loads could be found to examine. This equation could possibly be extended to include these loading conditions by including a shear term.

In addition to the prediction equations, the statistical analysis also indicated the parameters of major importance. This could be determined by observing F ratios given by the algorithm. The following four were found to be of major importance in both crack width and spacing:

1. Steel stress (f_s)
2. Concrete cover (COVER)
3. Width of beam (b)
4. Total depth of beam (h)

The effect of each parameter could be ascertained from the final equations. For example, crack width varies directly with steel stress

and inversely with the number of bars. Similar statements can be made concerning crack spacing also.

IV. DETERMINATION OF BOND STRESS DISTRIBUTION

The two basic quantities which need to be evaluated before crack widths can be predicted are bond stress distribution and effective concrete area. These two are interdependent and, therefore, if one is defined, the other can be reduced from the recorded data on crack widths. Since the steel stress can be determined in the laboratory and then converted to bond stress, it was decided to define the bond stress distribution first. To do this, an analytical and an experimental model were employed.

Analytical Model

The analytical model was a digital computer program using a finite element program developed by Wilson[6] for the analysis of axisymmetric solids. Wilson's program was amended to accomodate the Ngo and Scordelis[8] bond element which was discussed in the Section II. Additional logic was added to calculate bond stress along the steel and the total force in a concrete layer.

Input is by cards with the following order:

1. First card - month, day and year in first six columns without any blanks and in column eight the material number of the steel.
2. Second card - heading to identify the problem.
3. Third card - number of nodal points, elements, materials and pressure cards in I5 format, and in column 45, the number of approximations needed for the non-linear analysis.

4. Next cards - material properties for each material.
5. Next cards - nodal points and locations.
6. Next cards - element incidences and material number.
7. Next to last card - pressure card for load.
8. Last card - bond information; one (1) in column five if the force on a concrete layer is needed, and in the next ten columns, the number of concrete elements in a layer, and the number of layers both in I5 format; following this in F5.0 format the width of the concrete elements.

Output from the program includes the following:

1. Nodal displacements in the r- and z- directions,
2. Element stresses and strains in the r- and z- directions,
3. Principle stresses and their angle of inclination for each element,
4. Maximum shearing stress in each element,
5. Bond stress distributions,
6. Force in each concrete layer and
7. If Ngo and Scordelis' bond element is used, the force in that element.

The first three items listed are usual output and will not be discussed.

The fourth one above, maximum shearing stress, is easily calculated by dividing the difference between principal stresses in the r- and z- directions by two. This quantity was calculated because the photoelastic results are shearing strains, which can be con-

verted to stress quite easily.

Number five, bond stress distribution, is calculated by multiplying the difference in steel stress between two adjacent steel elements with constant r by the steel area. This force is then divided by the surface area of the steel giving a bond stress.

The sixth one, force in a concrete layer, is found by integrating the stress in a layer of concrete, (concrete elements with constant z- coordinate). The stress is first multiplied by the appropriate r-coordinate, then integrated using Simpson's rule extended to a power one less than the number of elements in a layer.

Number seven is determined only when the Ngo and Scordelis element is used. The bond force is determined by multiplying the net displacement of each end by the spring stiffness. This is done for both the r- and z- directions.

To model the bond between concrete and steel, a special type element was used. This bar bond element is shown in Figure 5. It is a thin cylinder around the steel, connected to the steel at one node and to the concrete at the node diagonally opposite. Material properties of this element are:

1. Modulus of elasticity - same as steel
2. Slope of plastic stress-strain curve — 0.001 times E_s
3. Yield stress - steel stress at the allowable bond stress of the concrete.

The bar bond element allows elastic action to take place at low loads, but as the load increases, the bond element "yields" and plastic deformation occurs. This can be handled in Wilson's program using a

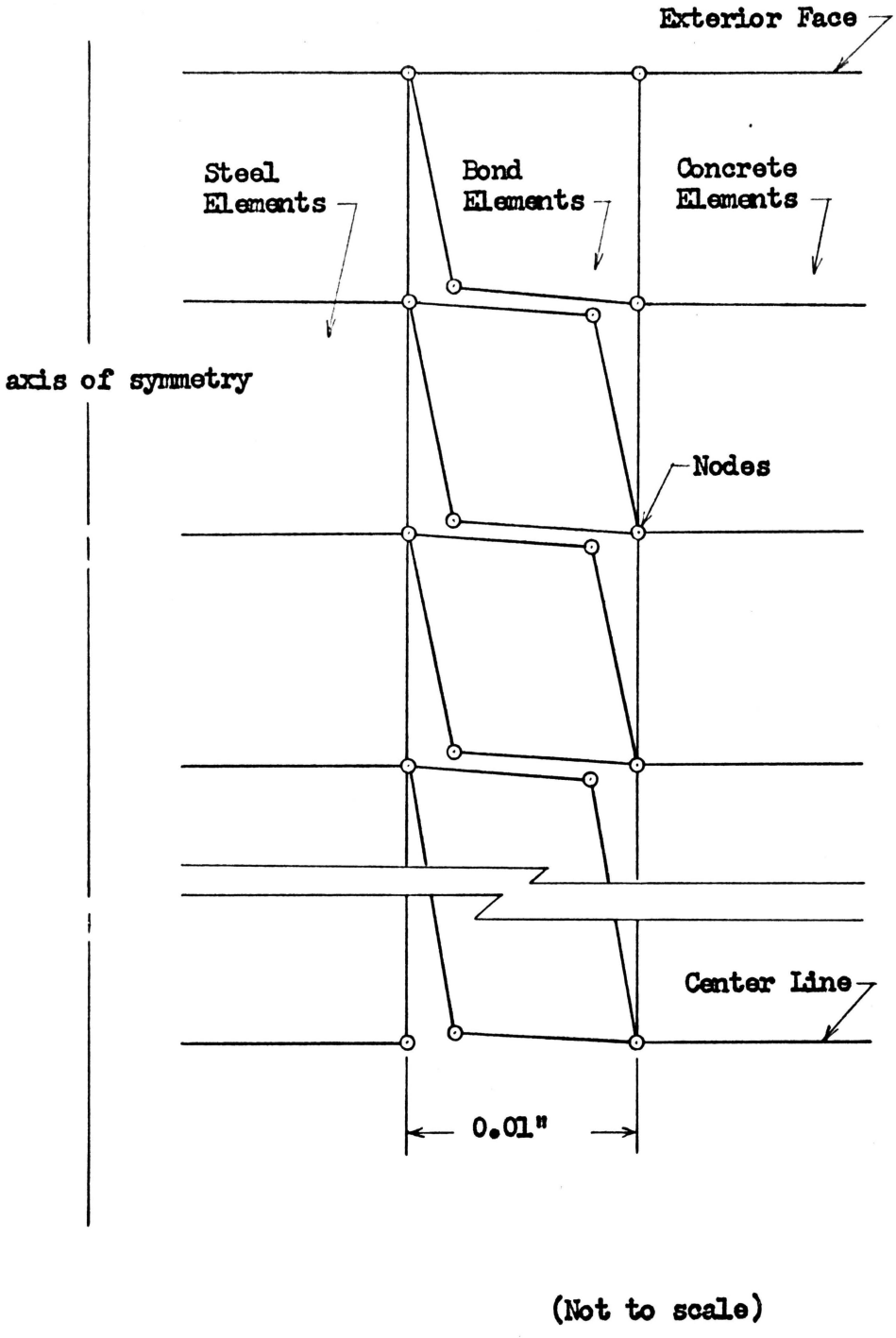

FIGURE 5. Bar Bond Element

direct iterative approach as defined by Zienkiewicz[17].

The direct iterative approach assumes that the effective strain is the second strain invariant; namely,

$$\bar{\epsilon} = \frac{2}{3}\sqrt{(\epsilon_1 - \epsilon_2)^2 + (\epsilon_2 - \epsilon_3)^2 + (\epsilon_3 - \epsilon_1)^2} \qquad (21)$$

and the effective stress is

$$\bar{f} = \frac{1}{3}\sqrt{(f_1 - f_2)^2 + (f_2 - f_2)^2 + (f_3 - f_1)^2} \qquad (22)$$

where the subscripts indicate principal strains and stresses. The procedure can be defined with the above expressions and the following steps:

1. Apply full load and calculate strains and stresses using elastic procedures.
2. New values of E and ν are determined for each element according to its state of stress.
3. An elastic analysis is performed with total load, and the new elastic constants found in (2).
4. Iterate steps (2) and (3) until desired accuracy is obtained.

Usually only four or five iterations were required for good results. This procedure is shown schematically in Figure 6.

The yield stress of the bond element is defined as the steel stress at the ultimate strength allowable for the concrete bond stress, but not greater than 3.0 ksi. The ACI 318-63 Code gives the allowable stress in the concrete for tension bars conforming to ASTM

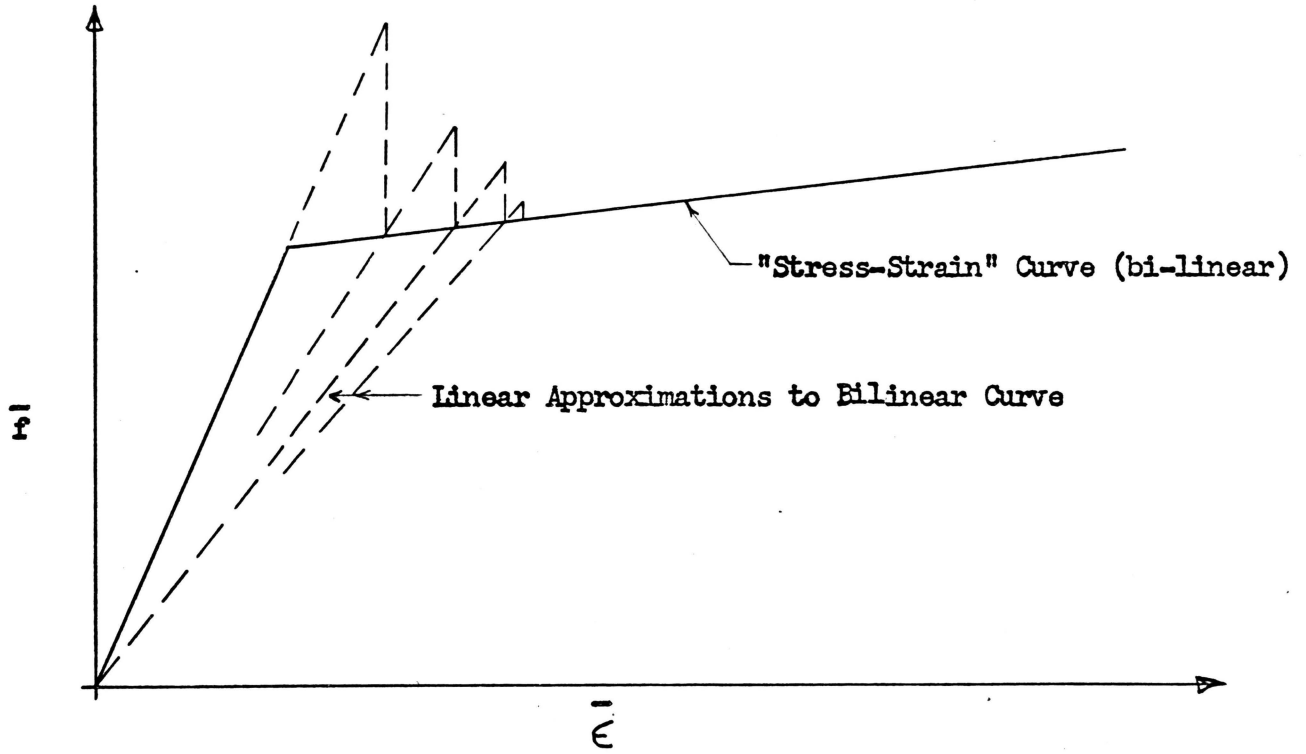

FIGURE 6. Direct-Iterative Approach to Non-Linear Bar Bond Element

A305 as $9.5\sqrt{f'_c}/D$ for other than top bars. To calculate the bond element yield stress, the allowable bond stress is multiplied by the surface area for a unit length and that force is divided by the steel area. For example, with the No. 11 bar:

$D = 1.41$ in. $\qquad A_s = 1.56$ sq. in.

$f'_c = 4075$ psi $\qquad$ Perimeter = 4.430 in.

the ultimate allowable bond = $9.5\sqrt{4075}/1.41 = 426$ psi

the bond force = 426 (1) 4.430 = 1890 lbs.

the steel stress = 1890/1.56 = 1212 psi

the bond element yield stress = 1.21 ksi < 3.0 ksi

The bond element yield values used in the theoretical model are:

No. 4 bar - 3.0 ksi

No. 8 bar - 2.4 ksi

No. 11 bar - 1.2 ksi

EXPERIMENTAL

The testing program was designed to verify the analytical model for bond transfer and also to evaluate the stiffness of the model bond element. Because of expense and time, a large statistical sample was not used. Instead the tests were set up in pairs of identical half-cylinders so results could be duplicated.

The basic model used was the axially reinforced concrete cylinder with tension applied to the reinforcement. To obtain concrete strains next to the steel, the cylinder was "split". This was done by forming only half of the cylinder around the steel bar (see Figure 7). Since the half-cylinder is unsymmetrical, bending in the steel bar is possible. This will be determined by a set of strain gages located at the center on each side of the bar. If a uniform bending moment diagram is then assumed, the other gage readings can be corrected for bending.

The dominant parameters in crack width and spacing were discussed earlier in reference to other investigations and also in the Section III. The most important are:

1. Steel stress
2. Concrete cover
3. The width of the beam
4. The total depth of the beam.

From these parameters, it was decided to use steel stress and concrete cover as parameters in this study. Varying steel stress was quite

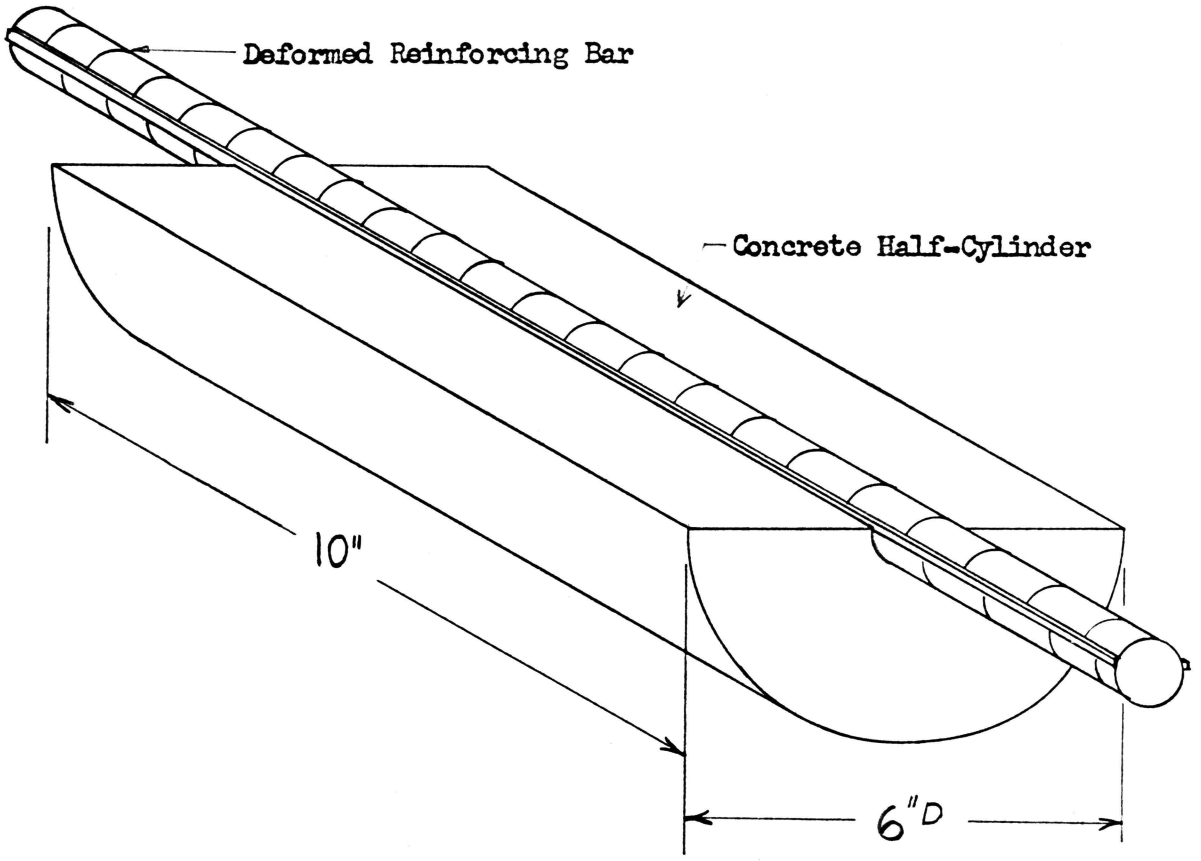

FIGURE 7. Test Sample - Concrete Half-Cylinder Axially Reinforced

simple using a testing machine. Three different size bars were cast in the same size half-cylinder, thus varying the concrete cover from 2.75" to 2.30".

Materials

The concrete mix is probably best described as a mortar (Table I). Small aggregate was used for two reasons:

1. Tension samples were needed and the standard tension sample is quite small.
2. The photoelastic coating is so sensitive that it picks up local strains around large aggregate and this confuses the total strain picture.

The reinforcing steel was obtained from a construction job on the V.P.I. campus. It has rusted slightly, but otherwise was in good shape. Three sizes were used — No. 4, No. 8, and No. 11. From each size three two-foot pieces were cut. Two were to be cast in half-cylinders, and the third was tested to obtain its stress-strain curve. All of these curves are plotted in Figure 8.

The No. 4 bars had all the ribs removed from the exterior side by filing and sanding. This was in preparation for strain gage application later. On the concrete side, the ribs were only removed at the center and only for a distance equal to the gage size. The No. 8 and No. 11 bars were milled to remove the ribs on the exterior side. This left a flat surface for strain gage application. On the concrete side, again as with the smaller bars, only a section at the center was cleared of ribs. The strain gage on the concrete side was affixed and

TABLE I

Concrete Mix Quantities

Retained on Sieve Number		Weight Pounds
10		0
16		41.8
30		50.0
50		7.6
100		.6
	Total	100.0
	Water	23.3
	Cement (Type III A)	34.5

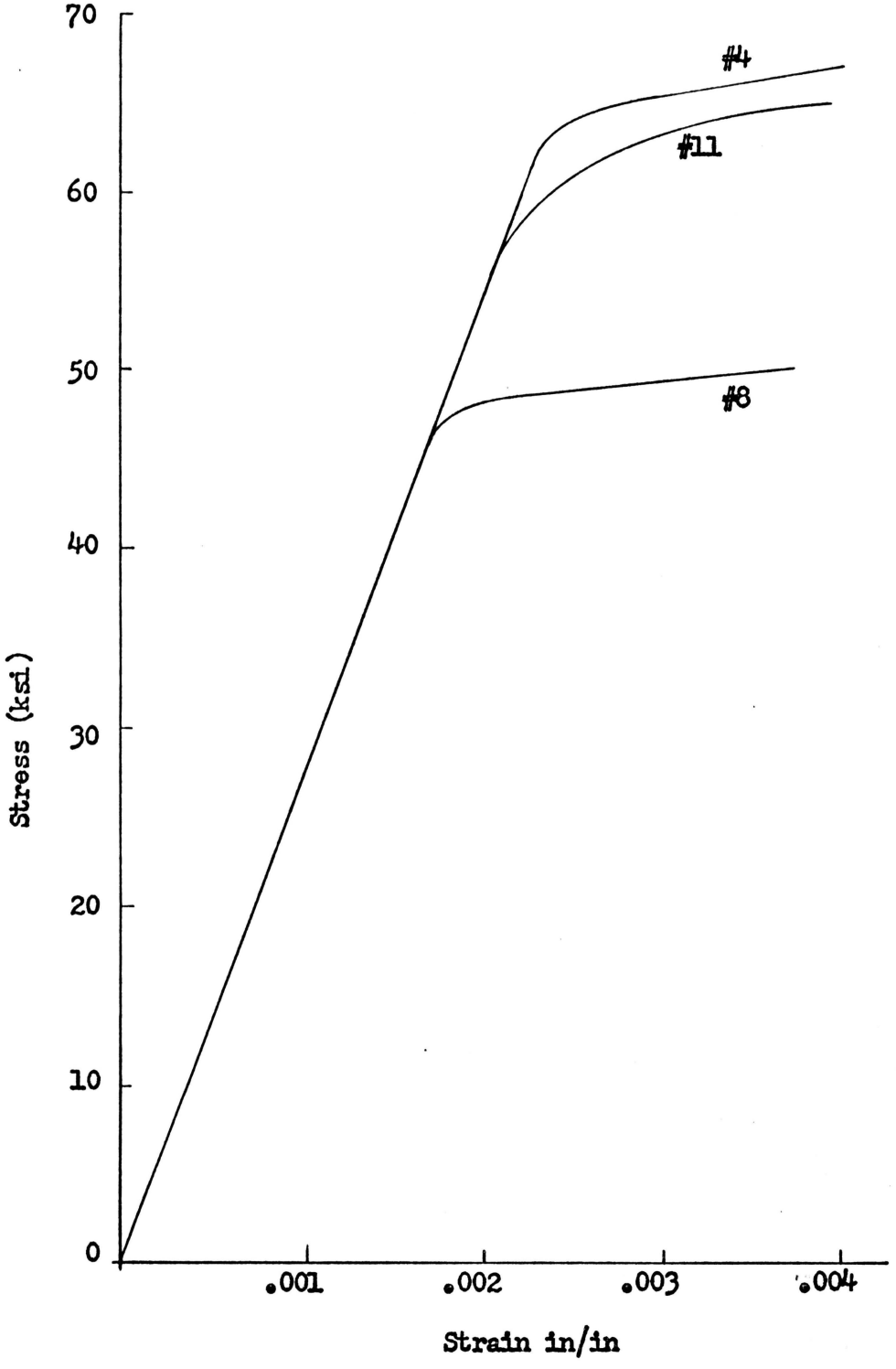

FIGURE 8. Stress-Strain Curves for Steel

water-proofed before casting.

An extra pair of No. 8 bars was cut and cast in half-cylinders to study the effect of a crack on the steel strain readings. No photoelastic material was used in these two tests and no strain gages on the concrete. There were 12 strain gages on the steel; one in the concrete and 11 outside the concrete. These gages were on one-inch centers beginning at one end and going the entire length. (see Figure 9). Preparation for the gages was the same as with the other half-cylinders.

Each half-cylinder was cast in a modified standard steel 6" x 12" mold with a plaster filler occupying half the area. The plaster filler was cast, dried and shaped by scraping and sanding. The steel was placed in a groove in the plaster and two pieces of Masonite were placed beside the steel on the flat surface. Care was taken to leave only half of the steel bar above the Masonite. A thin piece of cardboard was attached to the Masonite and both were taped to the plaster. The steel was also taped down to the plaster to hold it in place. The 6" x 12" steel mold was modified using a false bottom, leaving only ten inches of length.

The concrete was mixed by hand and two half-cylinders were cast at the same time, along with six compression cylinders (2" x 4") and eight tension samples. The forms were removed on all of the above after 24 hours in the moist room. They were then returned to the moist room. When removed from the moist room after another 24 hours, the first surface of the half-cylinder was rubbed with a concrete finishing brick to obtain a flat surface, and also to remove any fines

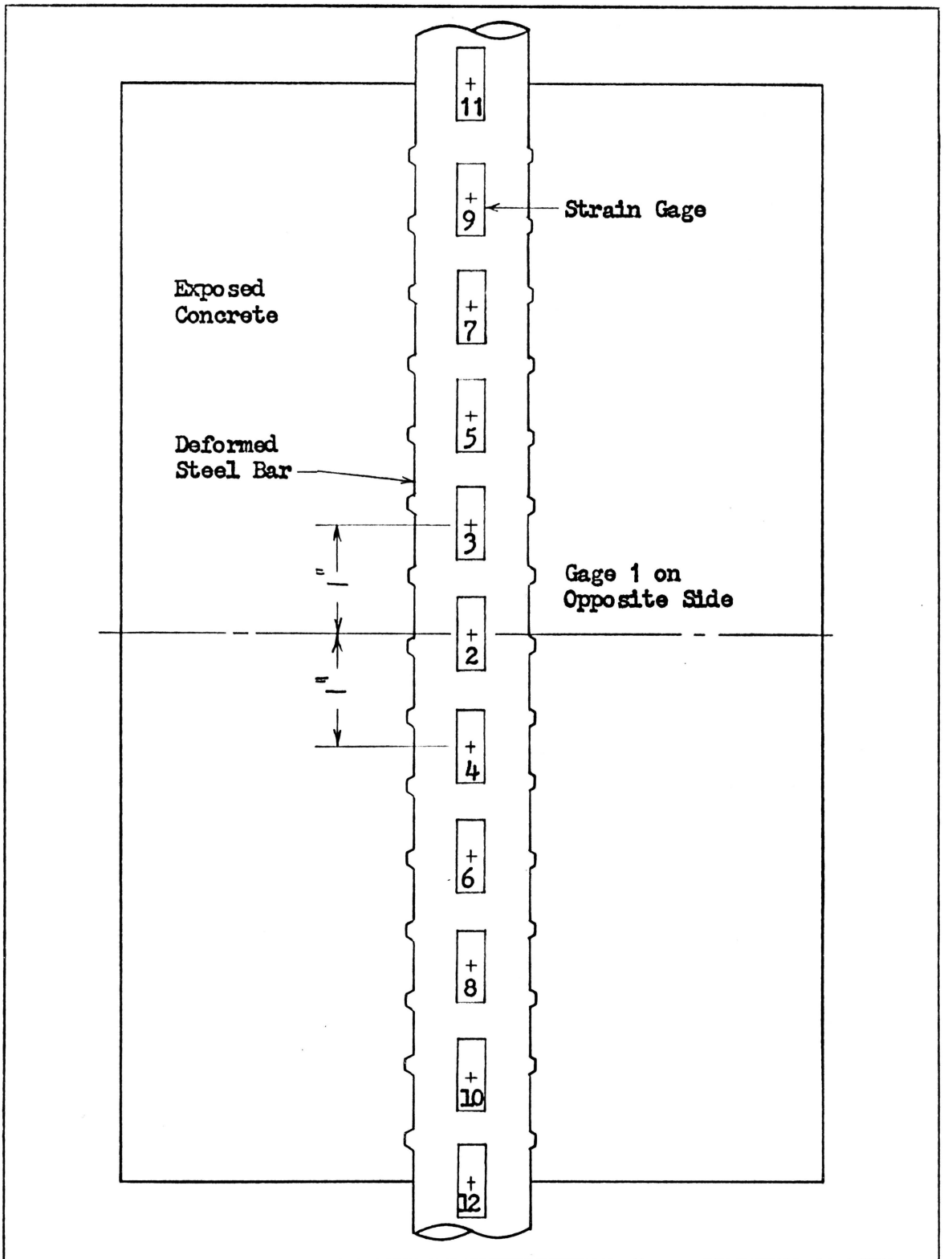

FIGURE 9. Instrumentation on Test 4 Half-Cylinder

that had worked to the surface. Sand paper was then used to get a smooth surface. All specimens were then allowed to air dry for about 30 hours.

The photoelastic material was obtained from Photolastic, Inc. and had the following properties:

1. 0.128 $\pm$ .002 inches thickness
2. K factor, 0.15
3. Fringe order, 593
4. Silvered back
5. Size 10" x 10"

The photoelastic sheets were cut to size to cover half the concrete surface (see Figures 10 and 11) with a quarter-inch gap between the steel and photoelastic sheet. Adhesive was spread over the concrete surface and allowed to dry for one and one-half hours. Then a thin layer of adhesive was spread over the dry adhesive and the sheet was pressed down until all air bubbles were worked out. Weights were applied on a piece of plyboard on the photoelastic sheets to assure good bonding.

Polyester base strain gages manufactured by University Precision Measurement Company were used to measure the steel stress and also as a check on the photoelasticity results. Two gage lengths were used, 0.28 and 0.40 inches. The shorter gages were used on the concrete, and the others on the steel. Approximate location of the gages is shown in Figures 10 and 11. Standard procedures were used in bonding the strain gages to the steel and concrete.

The strain gages for the tests without photoelastic material were

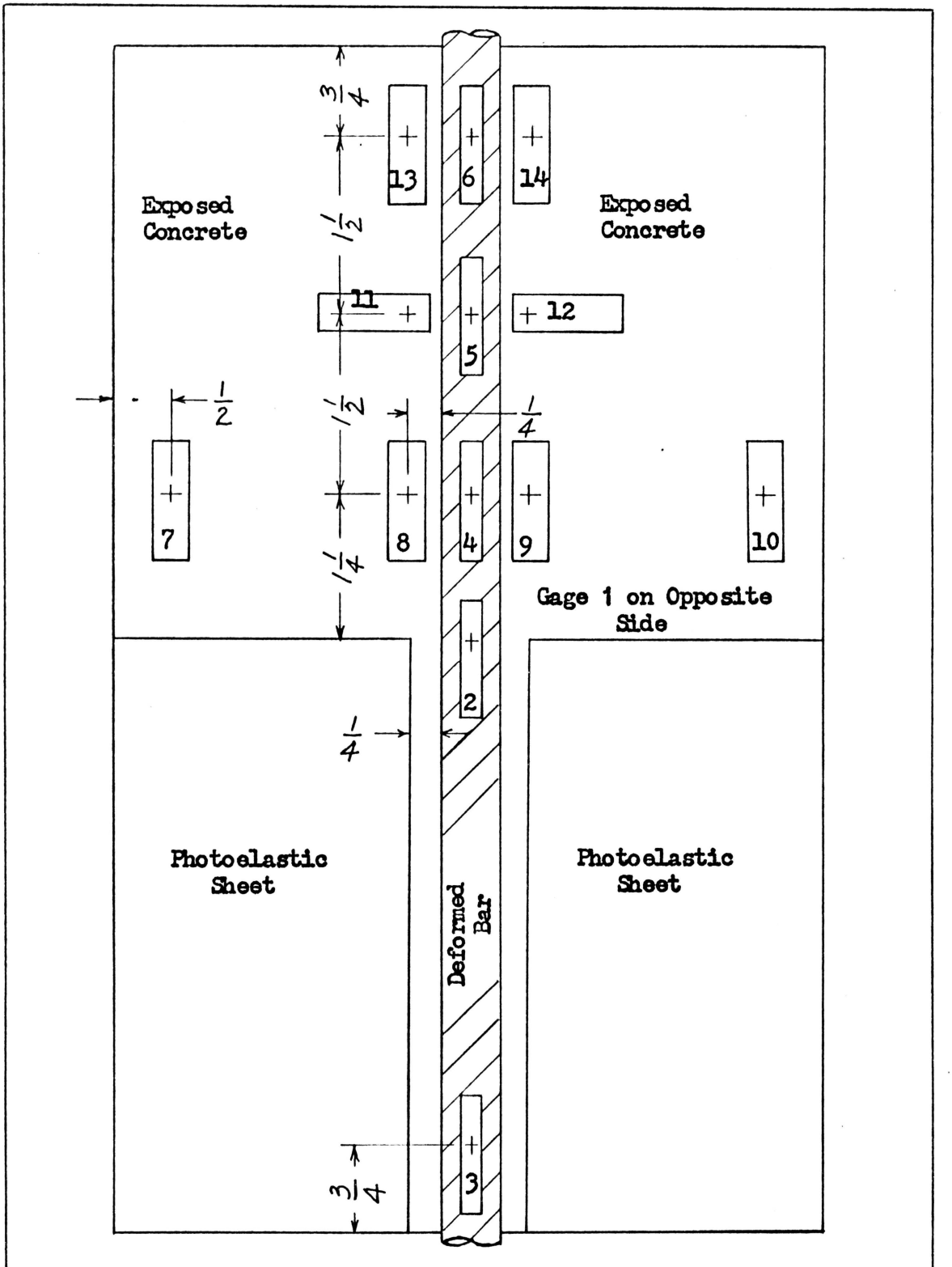

FIGURE 10. Instrumentation on Type A Half-Cylinders

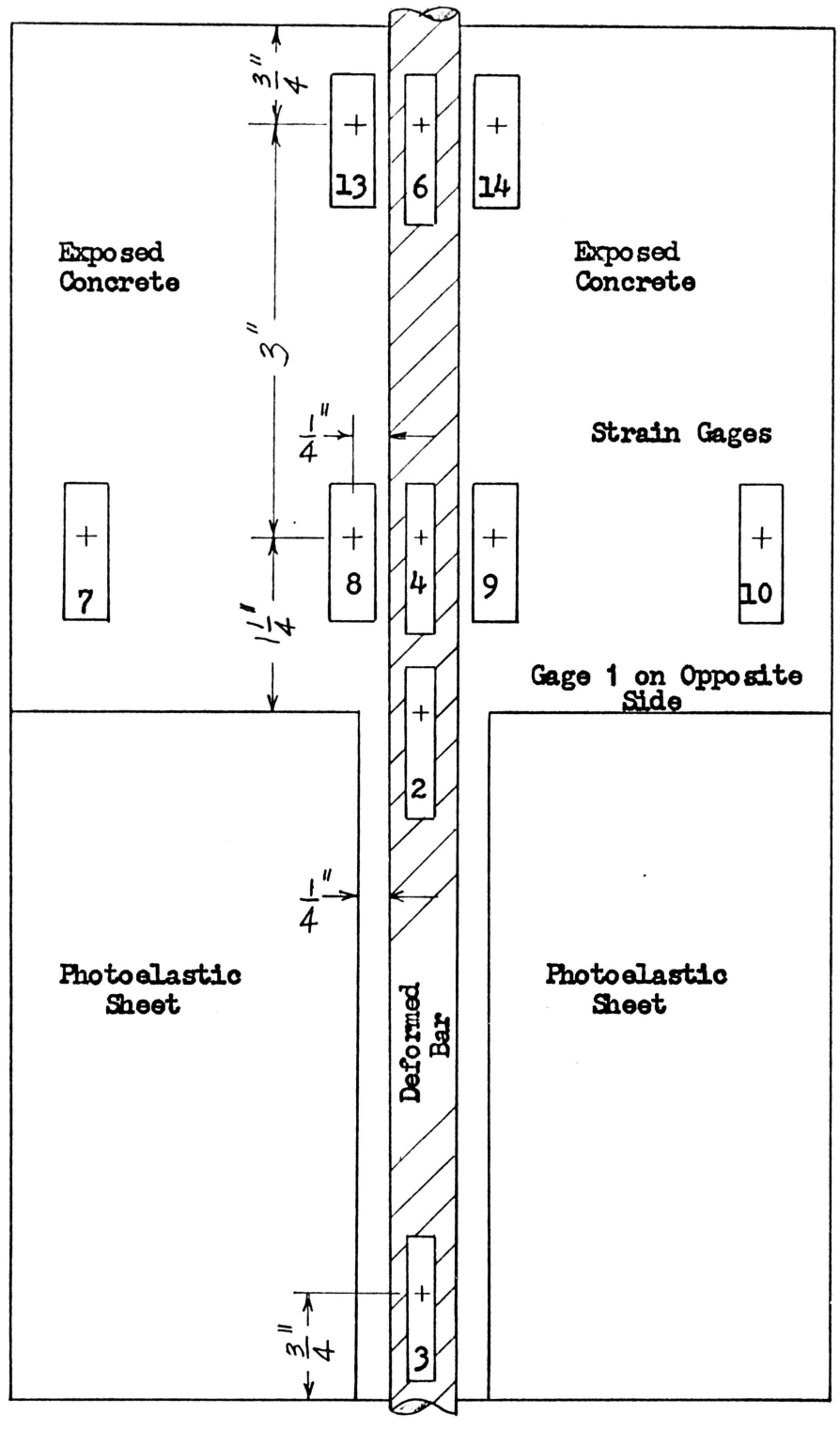

FIGURE 11. Instrumentation on Type B Half-Cylinders

obtained from BCS Associates, Inc. They were paper base gages with a gage length of 0.25 inches.

Table II contains a summary of data on each half-cylinder.

Testing Apparatus

Testing of the half-cylinders was done on a Tinius Olsen hydraulic machine with a capacity of 120,000 pounds. The steel was clamped in the jaws of the machine leaving three inches between the half-cylinder and the jaws. Tension was applied to the steel bar by moving one head of the machine with the other head fixed.

The strain gages were read using standard switching and balancing units. Only one compensating gage was used for all the gages on the steel and another compensating gage for the gages on the concrete. Each gage factor could be set on the recorder making the readings correct for each set of gages.

A portable polariscope was used to obtain photoelastic results. The light source was a 150 watt white light bulb. Three lenses were attached just in front of the light source in the following order beginning next to the source:

1. Polarizer
2. Quarter wave plate
3. Filter

The light passed through these plates and hit the half-cylinder and bounced back. The light then passed through another quarter wave plate and polarizer. This last set of plates is called the analyzer. On

TABLE II

Test Samples

Test Number	Number of Strain Gages on Concrete	on Steel	Photoelastic Material	f'_t	f'_c	Concrete E_c (2)	Steel f_y	E_s
1A	8	6	Yes	0.586	4.324	3.788×10^3	65.0	25.0×10^3
1B	6	5	Yes	0.586	4.324	3.788×10^3	65.0	25.0×10^3
2A	8	6	Yes	0.603	4.828	4.004×10^3	47.5	27.8×10^3
2B	6	5	Yes	0.603	4.828	4.004×10^3	47.5	27.8×10^3
3A	8	6	Yes	0.660	4.075	3.678×10^3	57.0	27.8×10^3
3B	6	5	Yes	0.660	4.075	3.678×10^3	57.0	27.8×10^3
4A (1)	0	12	No	0.580	5.679	4.340×10^3	47.9	31.5×10^3
4B	0	12	No	0.580	5.679	4.340×10^3	47.9	31.5×10^3

(1) 4A was slotted around its circumference on the center line of the half-cylinder to induce a crack.

(2) $E_c = w^{1.5}\, 33\sqrt{f'_c}$

this particular model, the analyzer was about 15" in diameter with the quarter wave plate on one side and the polarizer on the other. The above setup was for a circular polariscope which gave the best picture of the maximum shearing stress fringes. A sketch of this setup is shown in Figure 12.

To record the fringes, a 35mm, single reflex lens camera was used with a 50mm lens and Kodacolor X film. The camera was set on a tripod just behind the analyzer. A color chart with the primary colors was used to establish a reference for analysis. About three pictures were taken at each load of zero, half of the steel yield stress and full yield stress.

A picture of the total test setup is shown in Figure 13.

Test Procedure

The half-cylinders were placed in the testing machine and all gages connected to the recorder and zeroed. The polariscope was then set up as close to the half-cylinder as possible. The camera was placed just behind the analyzer and adjusted to obtain the proper picture. The tests were conducted at night when the testing room was dark with the lights off. The only light source was the light on the polariscope.

Each test began when pictures of the color chart were taken (see Figure 14). The next three pictures were initial, no load shots for referencing the later pictures. The initial picture from Test 2B is shown in Figure 15. After these pictures, the load was increased in steps of about 15 percent of yield stress up to the yield stress

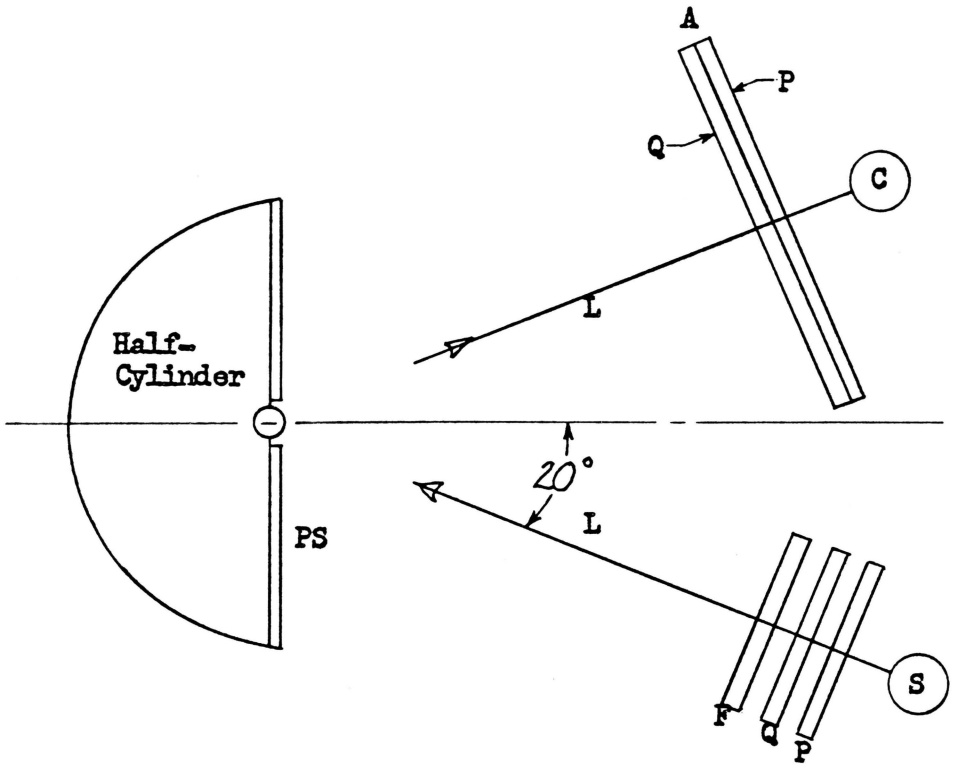

Notation

A - Analyzer
C - Camera
F - Filter
L - Light Wave
P - Polarizer
PS - Photoelastic Sheet
Q - Quarter Wave
S - Source

FIGURE 12. Photoelastic Setup (Circular-Crossed Polariscope)

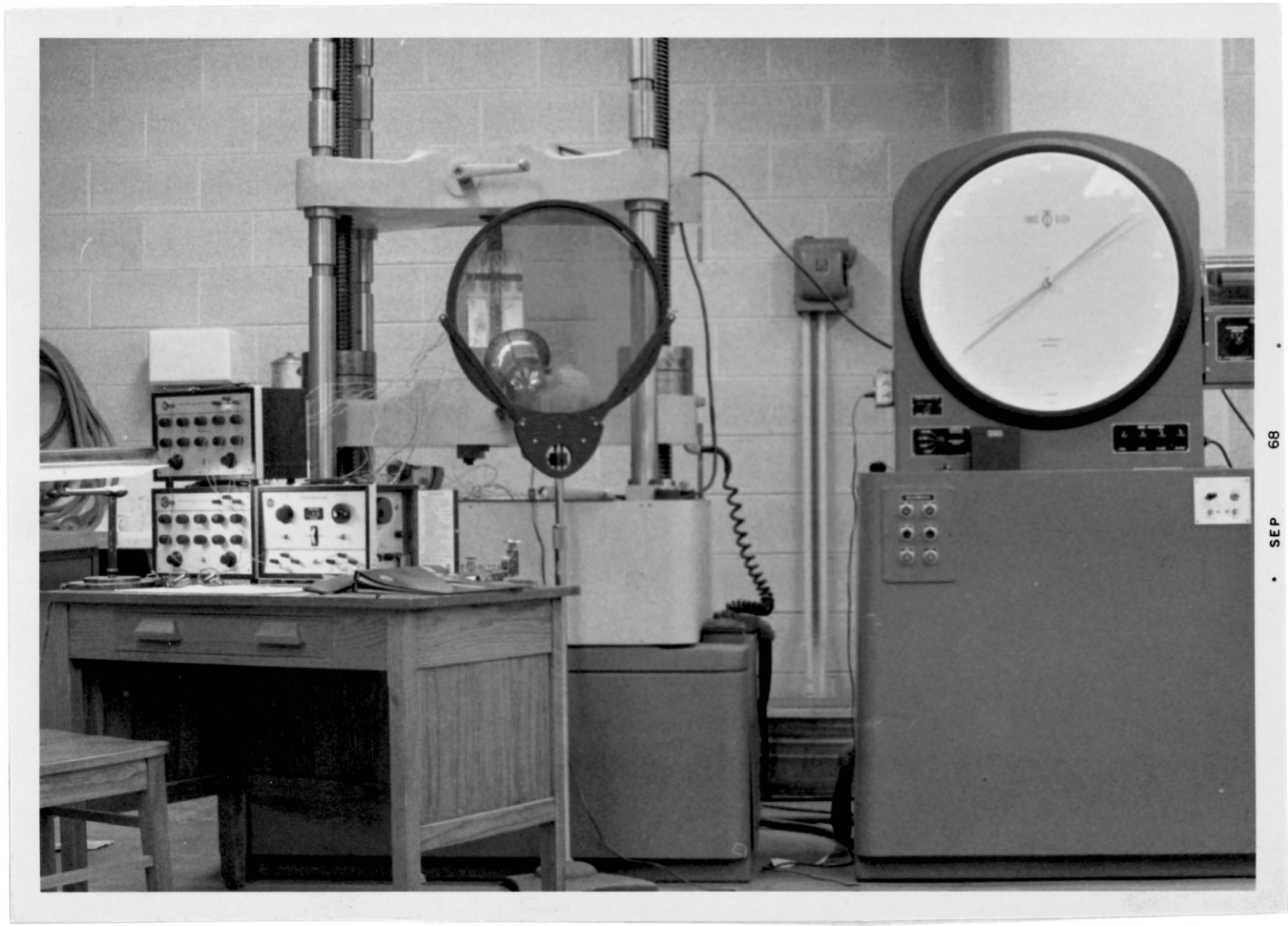

Figure 13. Complete Test Setup

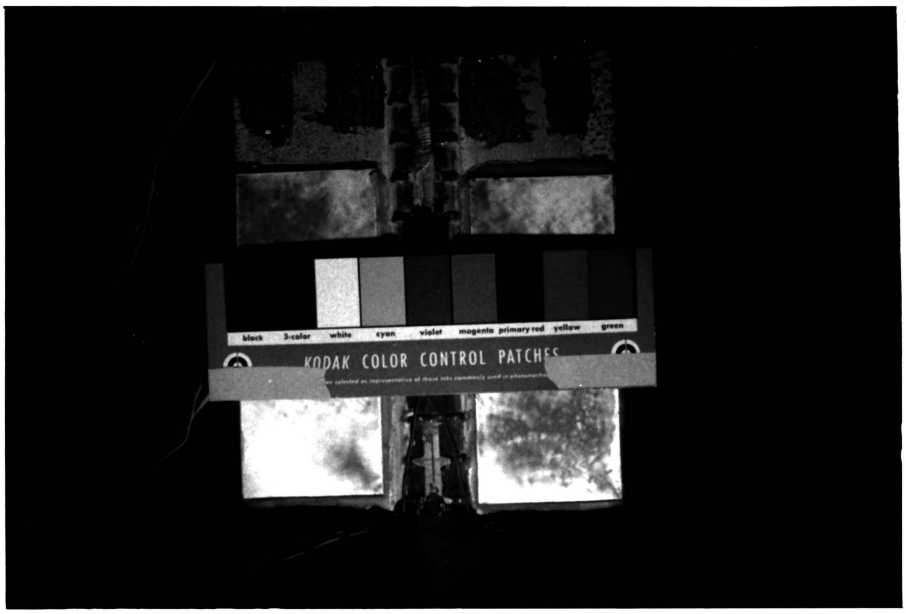

SEP 68

Figure 14. Color Chart

Figure 15. Zero Load Picture Test 2B

Figure 16. Final Load Picture Test 2B (f_s = 43.8 ksi)

of the steel. Pictures were taken at about half of yield and again at yield stress. The final picture from Test 2B is shown in Figure 16. The strain gages were read and recorded at each step. If something unusual happened, a picture was taken to record it. For example, in Test 3A a crack formed behind the photoelastic sheet. This gave a very interesting fringe pattern which is shown in Figure 17.

Two half-cylinders were tested each night and recorded on the same roll of film. The same procedure was followed for each test. After each pair of tests, the film was developed but not printed. The negatives were analyzed using an enlarger which projected the negative onto a flat surface. The enlarger was adjusted so that the projection was actual size. A piece of plain paper was used for the projection surface and the color pattern was traced onto it. First, the initial fringe pattern and then the final pattern were traced. With these two tracings and the properties of the photoelastic material, maximum shearing strains could be determined. This method was used on all the tests with the photoelastic material. The shearing strains were then converted to shearing stresses for comparison with the analytical results.

Test 4A was slightly different in that the load was increased on the half-cylinder until it cracked. The location of the crack was predetermined by a slot. After cracking, the load was reduced to zero and the half-cylinder reloaded following the same schedule as the other tests. Test 4B was exactly like 4A but with no slot.

The strain gage data was recorded in micro-inches per inch. The data from the gages on the steel were corrected for bending in the

Figure 17. Fringes at Crack Test 3A

plane normal to the photoelastic surface by subtracting the bending strain recorded by two gages in the center of the half-cylinder. This, of course, assumes a constant bending moment diagram along the steel which seems reasonable. The only bending corrected for is the bending in and out of the concrete. Gages symmetric about the center line were averaged since they would normally experience the same strain. These adjusted strains were then compared with the analytical results. A complete set of data for each test can be found in Appendix B.

Comparison of Models

The comparison of the two models is a very important step toward the final objective of this research. If the analytical model can be verified, then it can be used to generate data to determine the bond stress distribution. This section will be divided into four parts, the first three corresponding to the three different quantities measured in the experimental tests, and the fourth a summary.

Steel Strain Gage Results

The strain gages on the steel gave very consistent results between the A and B half-cylinders in each test. In the first three tests, the steel distribution was a little different from what was expected. The expected distribution is shown in Figure 4 between either pair of cracks. Test 4 was introduced to determine if a crack which forms late in the test has the same effect as an initial crack. Test 4A had the initial crack and Test 4B was identical to 2A and 2B except for slight

differences in f'_c and E_s. Since the strain gages values were averaged across the axis of symmetry, only half of the distribution is presented. In Figure 18 it can be seen that there was a large difference between the cracked and uncracked half-cylinder. This indicates that the strain distribution from the first three tests need not be exactly like that in Figure 4. If the length of the half-cylinder had been equal to about the average crack spacing, then the steel strain distribution would be like Figure 4.

The results of the third test are plotted in Figure 19. The points were obtained by correcting the stresses and strains from 3A and 3B to some central stress. For example, in 3A a stress level was 28.46 ksi and in 3B it was 28.08, therefore, the A strains were rounded off to 28.00 and multiplied by 28.00/28.46, and the B strains by 28.00/28.08. This gave two sets of data for averaging at a stress level of 28.00 ksi. In Figure 19 the results of the comparison between the experimental and analytical distributions are shown. Figures 20 and 21 show the comparison of Tests 1 and 2.

Photoelastic Results

The photoelastic results were on the whole only fair, however, some specific tests were quite good. No results could be obtained from Test 1A or 1B with the No. 4 bar. There was not enough strain in the concrete to show in the photoelastic material. The only exceptions being at the steel deformations where some strain concentrations could be seen. In Tests 2A and 2B, the results were complicated by the many strain concentrations around the steel deformations. Figure 22 shows

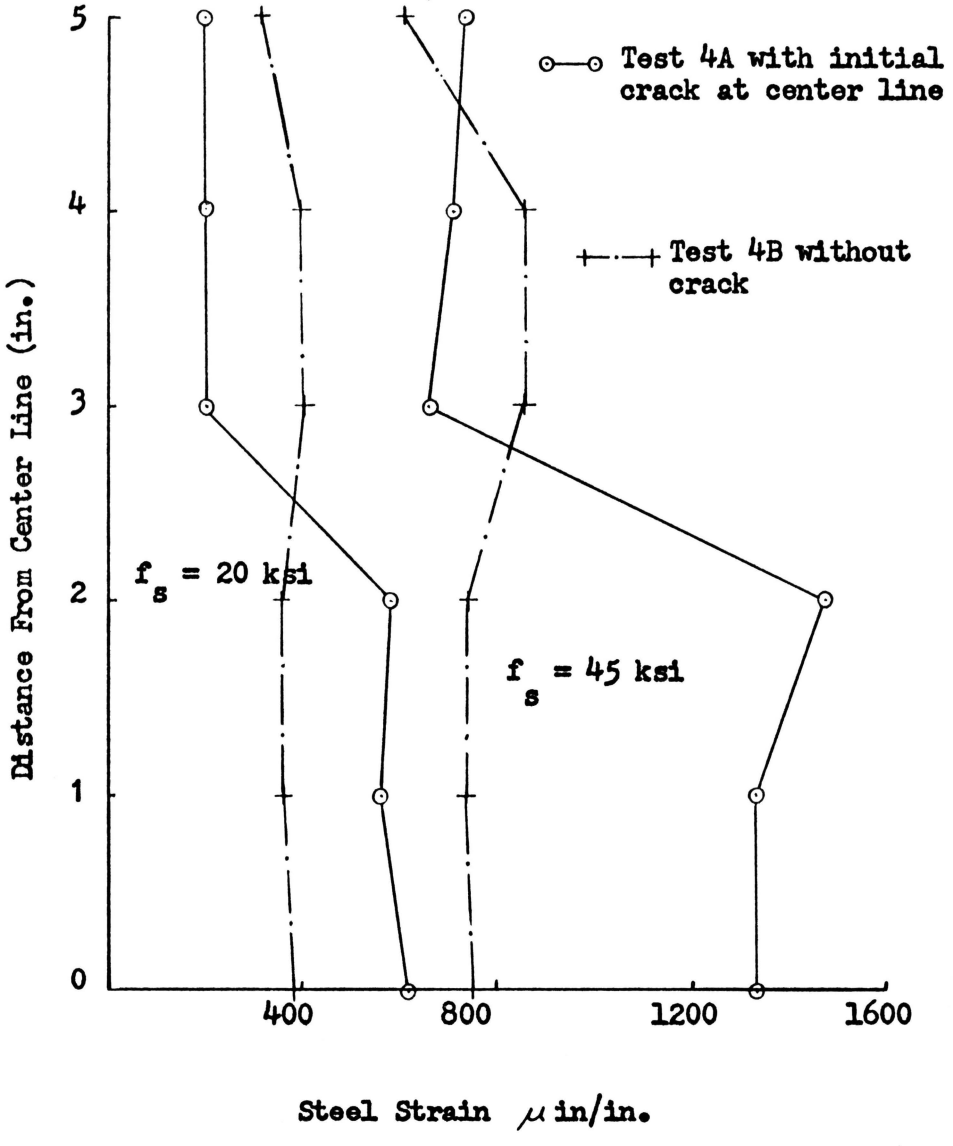

FIGURE 18. Steel Strain Comparison: Test 4A with 4B

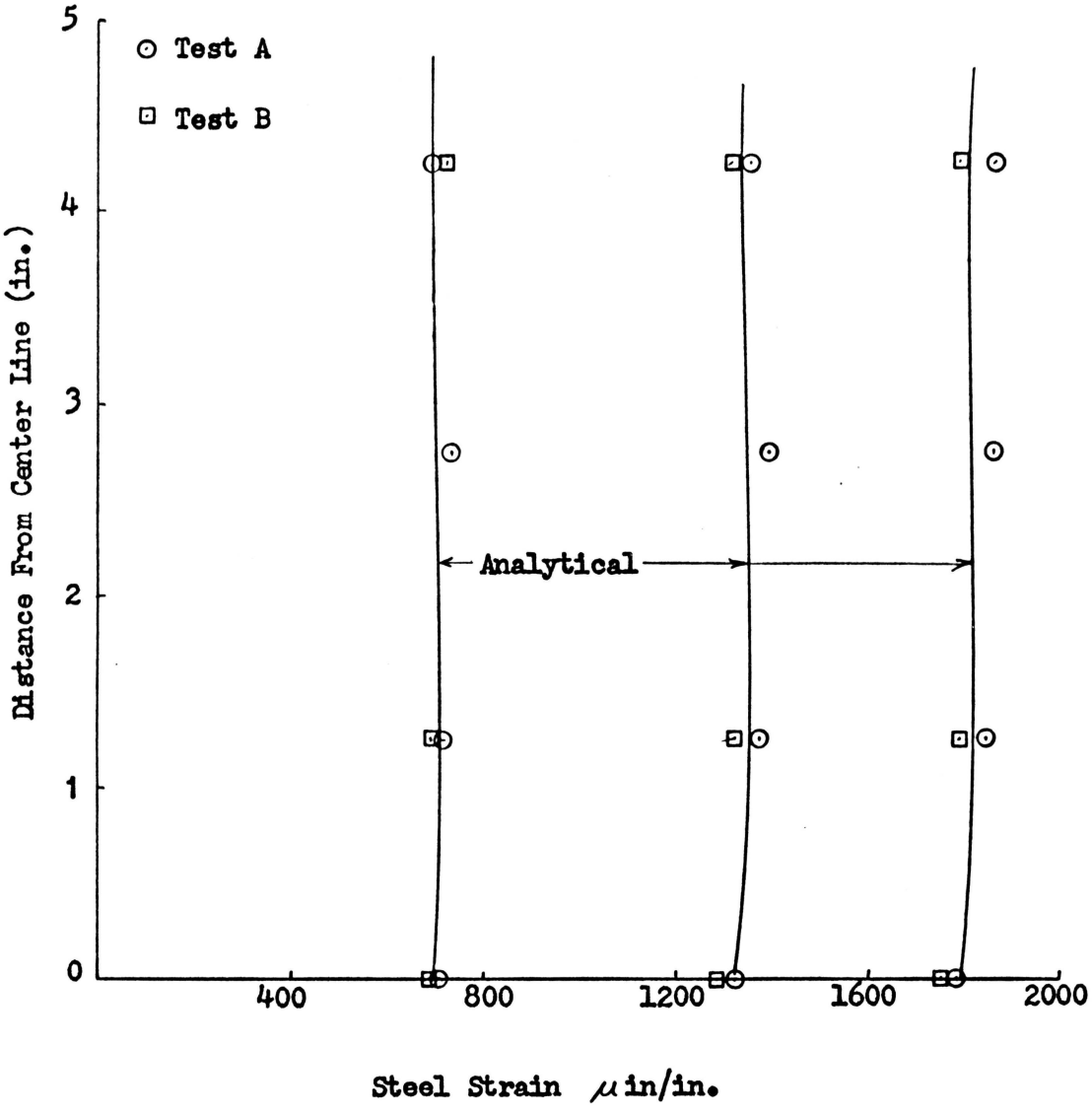

FIGURE 19. Steel Strain Comparison: Tests 3A and 3B

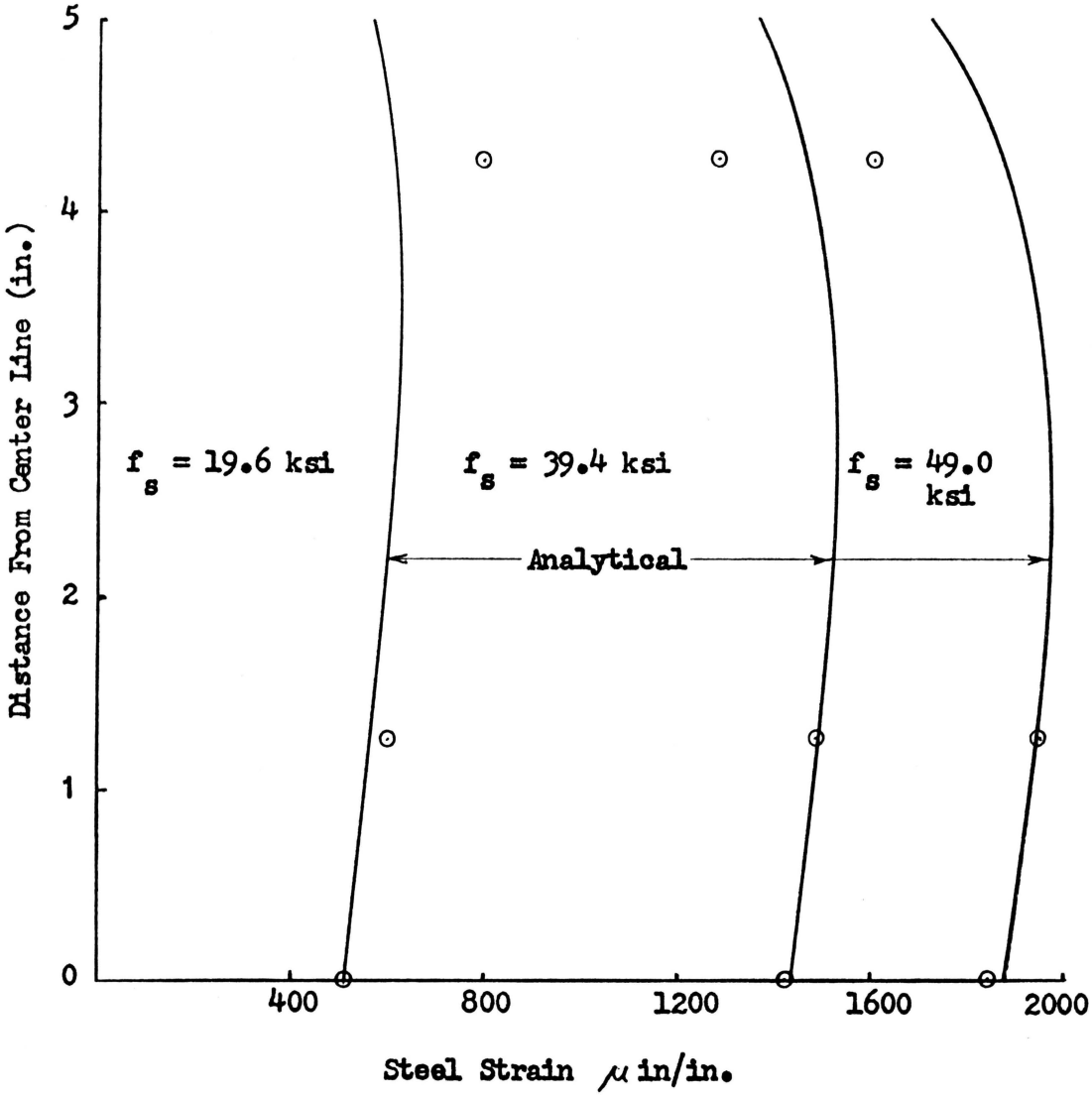

FIGURE 20. Steel Strain Comparison: Test 1B

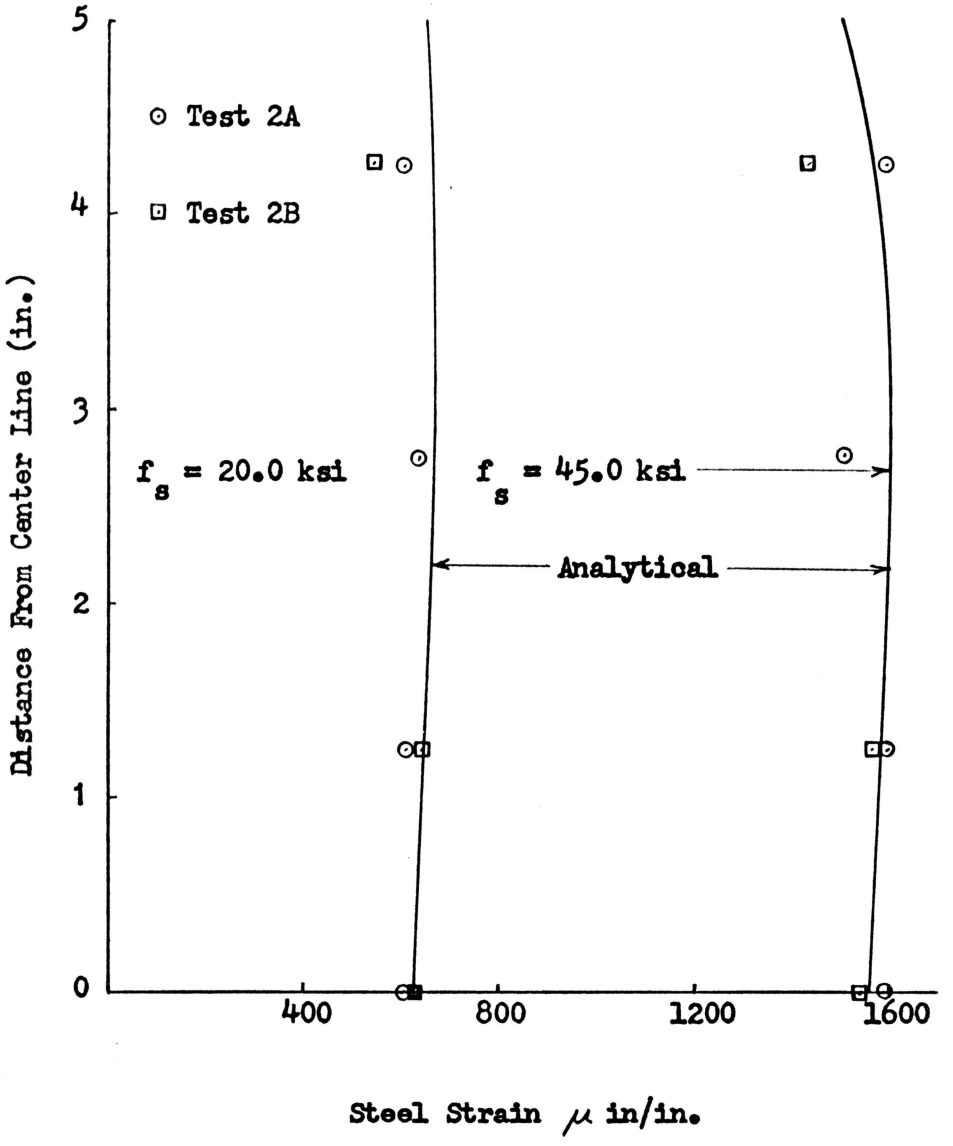

FIGURE 21. Steel Strain Comparison: Test 2A and 2B

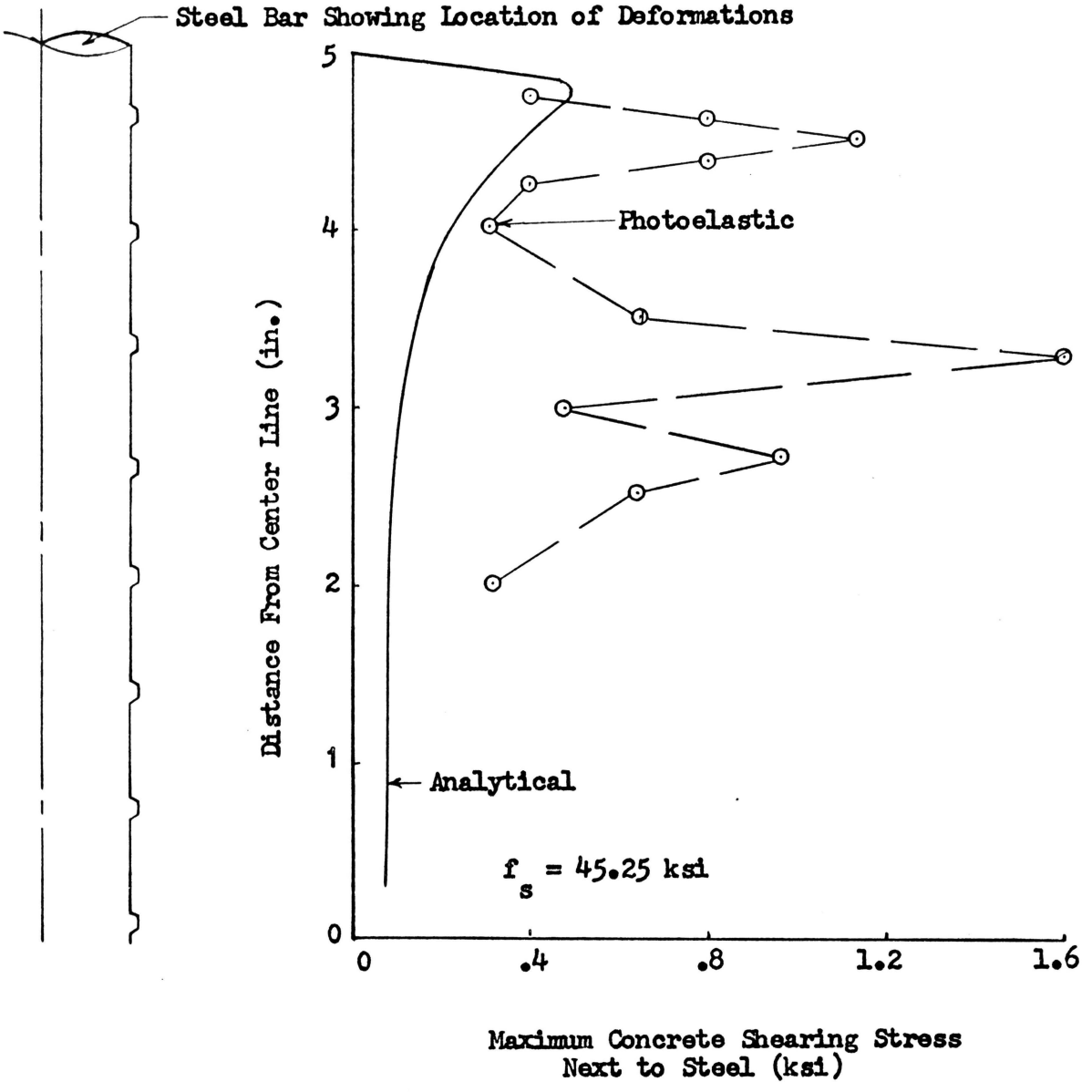

FIGURE 22. Photoelastic Comparison: Test 2A

the results of Test 2A and Figure 23 shows the results of Test 2B. The right and left sides were averaged to obtain the points shown in both of the above figures. Test 3A and 3B were the most successful with the photoelastic material. Figures 24 and 25 show the results of Test 3A and 3B, with right and left sides again averaged to get the photoelastic points.

There seem to be three reasons for the photoelastic problems. The first is the basic problem of the non-homogenity of the concrete. Pockets of incompletely mixed material cause strain concentrations which confuse the fringes. The second is that the photoelastic sheet is not sensitive enough to reflect the small strains in the concrete. The photoelastic sheet used is the most sensitive standard sheet available commercially. More sensitive sheets could be obtained on special order, but their thickness may prohibit their usefulness. The third is that the photoelastic material was too sensitive near the steel. Next to the steel, large strain concentrations at the deformations were present and tended to confuse the total fringe pattern.

The numbers obtained from the photoelastic results are subject to many errors, such as:

1. Error in thickness, $\pm$ 1.5 percent
2. Error in fringe order, $\pm$ 1 percent
3. Error in distinguishing colors from the negatives
4. Error in putting a number on a color since usually only whole fringes were observed.

Even with this error, the stress patterns obtained were usually quite accurate. With this in mind, the experimental results compared

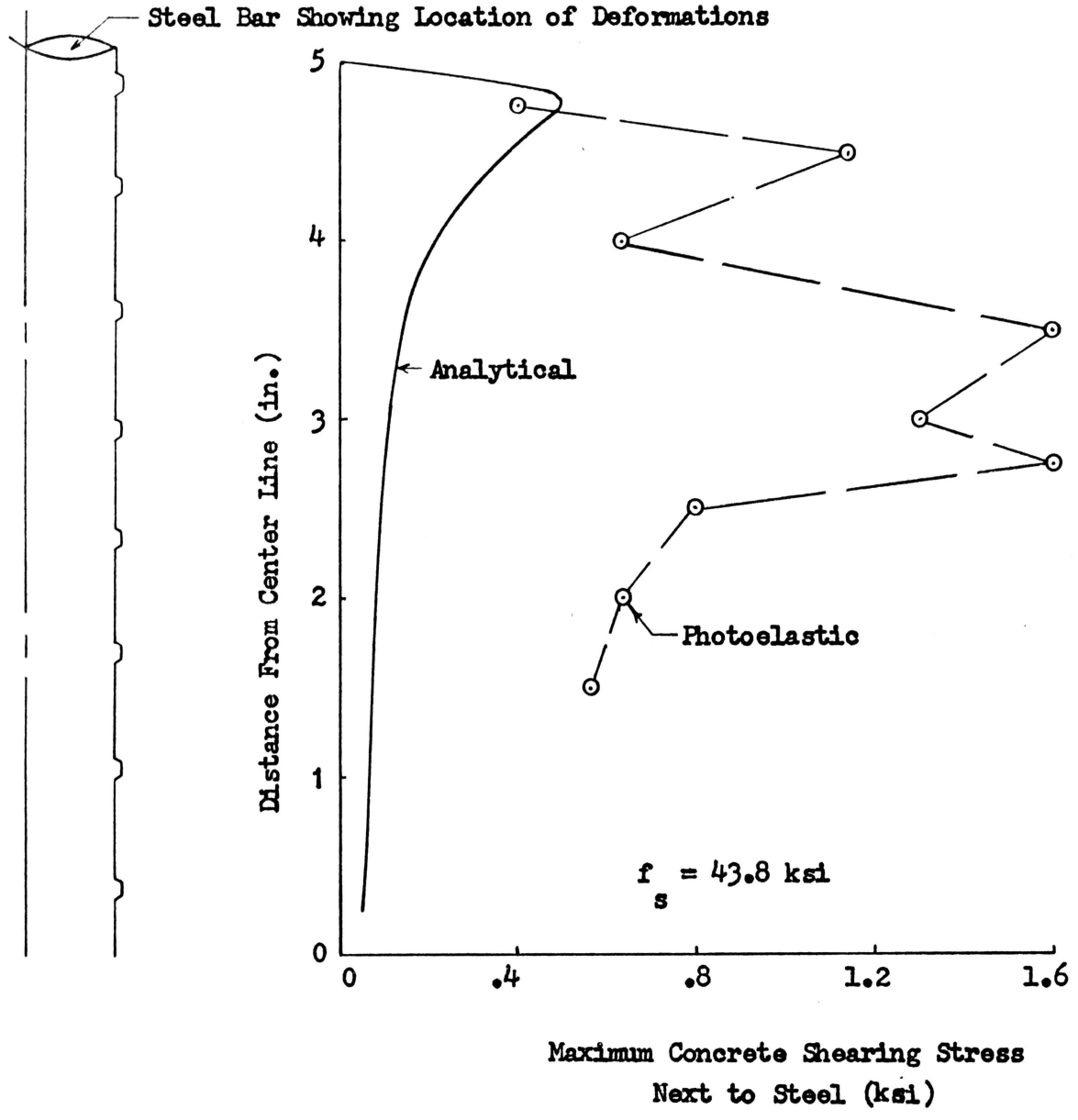

FIGURE 23. Photoelastic Comparison: Test 2B

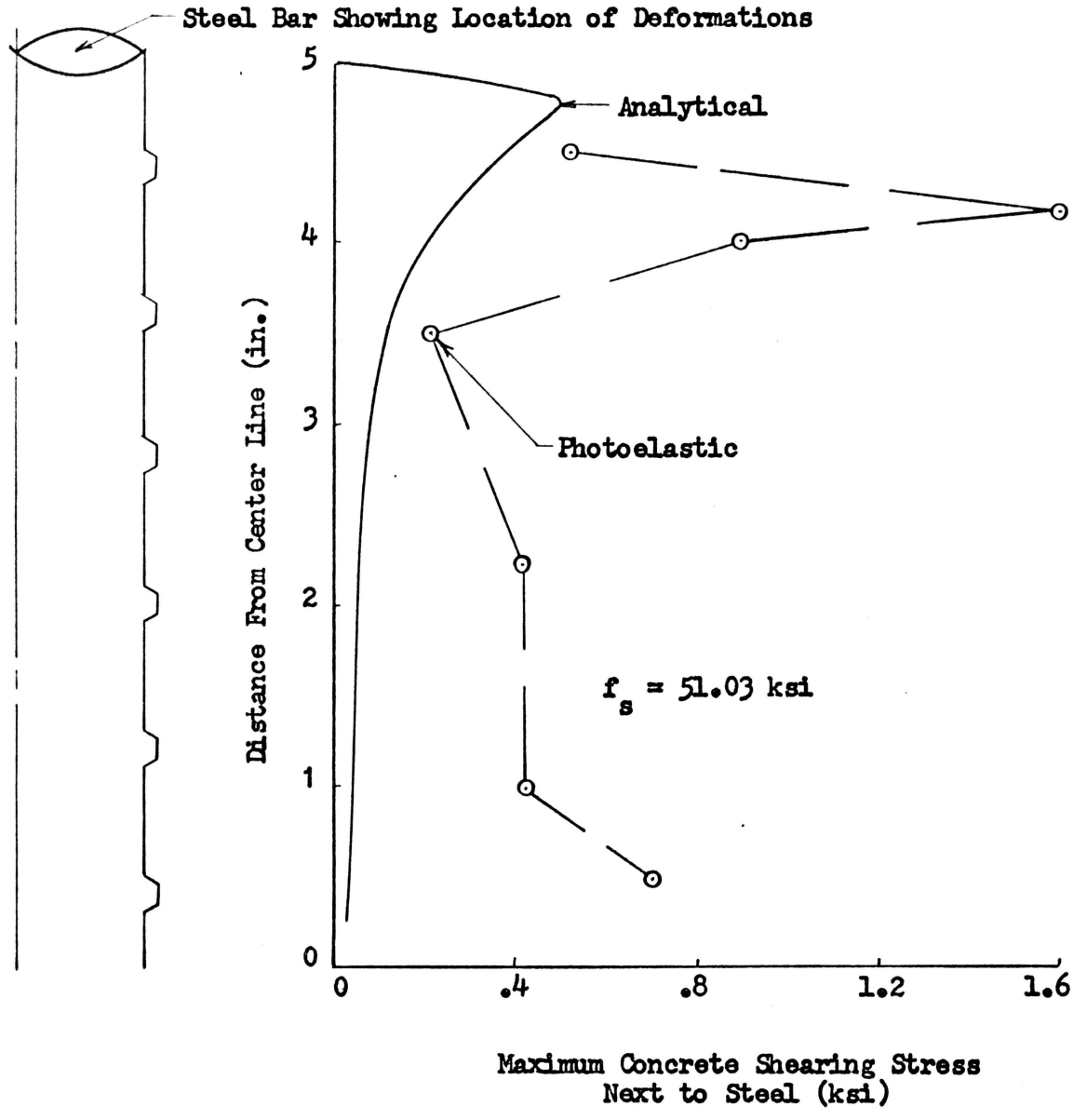

FIGURE 24. Photoelastic Comparison: Test 3A

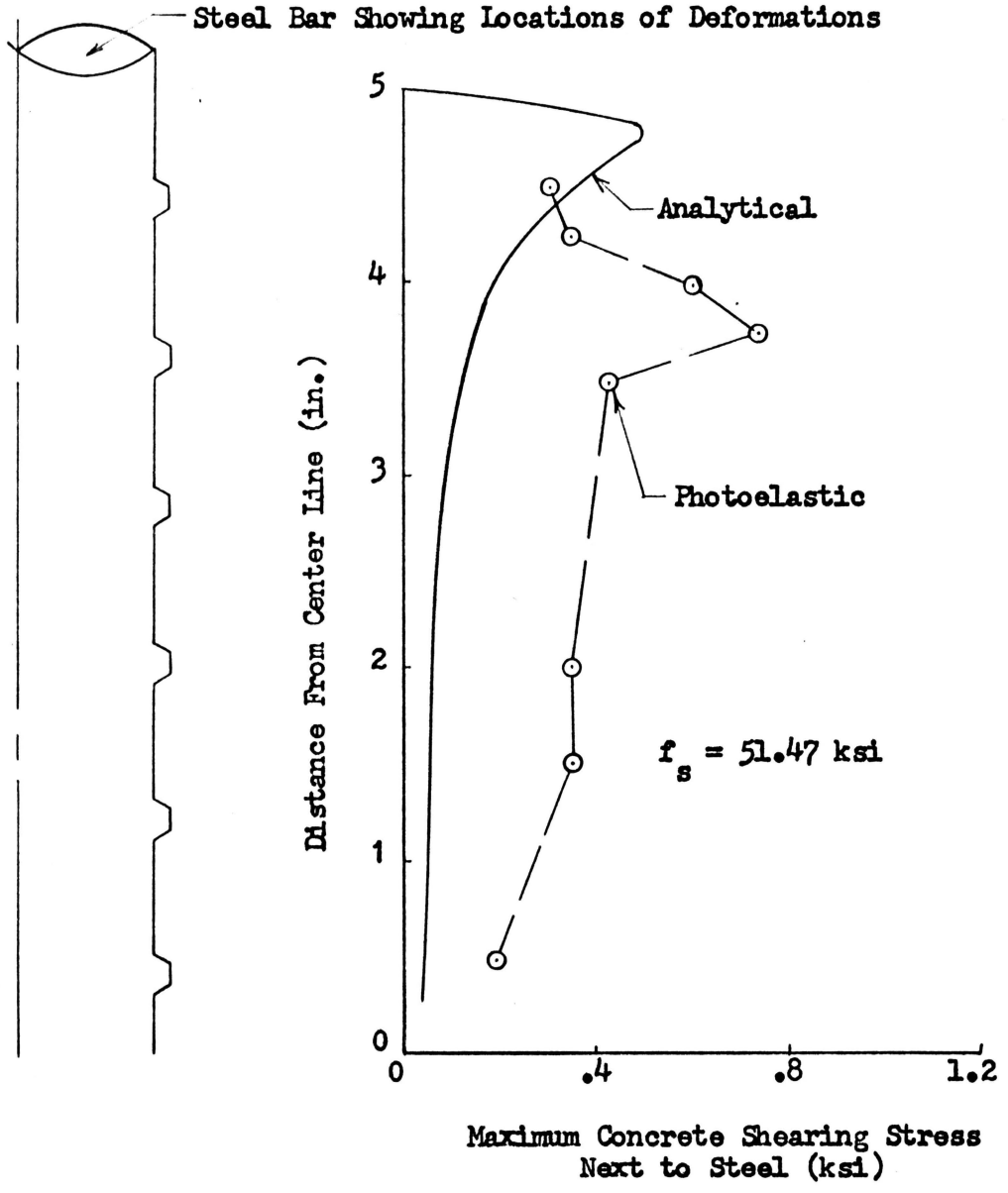

FIGURE 25. Photoelastic Comparison: Test 3B

favorably with the analytical model.

Concrete Strain Gage Results

The strain gages on the concrete were to be used as checks on the photoelastic results and also as points of reference for the theoretical model. None of the gages gave reasonable results. There seem to be a number of reasons for these poor readings. One, is the non-homogenity of concrete as discussed above. Other problems are the strain concentrations around the steel deformations. These cause some gages to record very high strains and yet adjacent gages record only small strains. Another problem is the wedging effect of the steel deformations as they try to slip through the concrete.

Some very questionable tensile strains were recorded in the concrete. Gage 7 in Test 2A recorded a tensile strain of 0.02 in/in. and Gage 13 recorded 0.01 in/in. in Test 3B. In both cases, the symmetrical gage recorded reasonable values. Because of the above problems, the concrete strain gage results were not compared with the analytical model.

Summary

Good comparisons have been made between the experimental and analytical steel strains, but concrete strains could not be compared. For this reason, comparison was made between the analytical surface deformations and the surface deformations measured by Broms[7]. In Part II of his article, he presented, in figure form, the surface deformation of a cylinder six inches in diameter and eight inches long,

reinforced with a No. 8 bar. Figure 26 shows the comparison and also gives more information about the test cylinder. Since good agreement is shown here also, the analytical model can be assumed correct.

In obtaining an equation for the bond stress distribution, the analytical model was used to vary steel stress and the cover. The steel stress was varied from 25 to 40 ksi in 5 ksi steps. The cover had values of 1.0, 1.5, 2.0, 2.5 inches and x varied from 0 to L/2. A total of 96 points were calculated and used as data in Heterick's[16] algorithm which was discussed in Section III. The bond stress equation from this algorithm was

$$u_x = 0.000539(f_s)^{1.36} (COVER)^{-0.0034} (x)^{-0.245} \qquad (23)$$

Since the exponent on COVER is so small, it was dropped from the equation. Therefore, the final equation at this point was

$$u_x = 0.000539(f_s)^{1.36} (x)^{-0.245} \qquad (24)$$

This equation will be adjusted when the final comparison is made between predicted and actual crack widths.

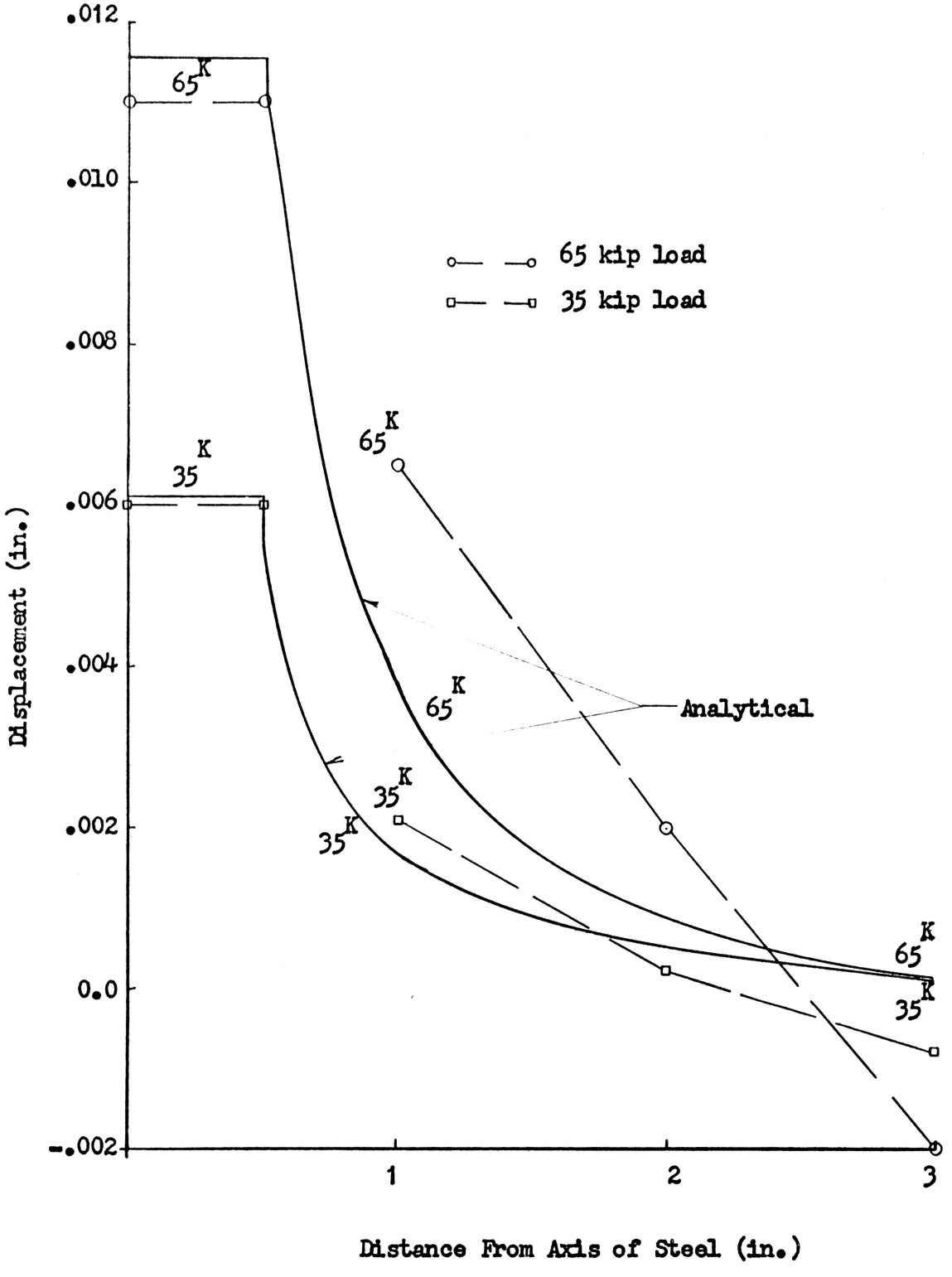

FIGURE 26. Comparison of Surface Deformations: Reference 7

V. DETERMINATION OF EFFECTIVE CONCRETE AREA

The limit of the concrete area beyond which the bond stress has little effect is needed in the development of a prediction equation for crack width and spacing. Two approaches were taken to define this limit. The first, and simplest, was to assume that this effective area is a constant. The second was to assume it is a function of x and f_s.

Constant

Many investigations have defined the effective concrete area A_e as the largest concrete area that is symmetric around the steel. This in a rectangular beam is equal to $2\left[b(h-d)\right]$.

In the model used in this investigation, the above definition does not apply; therefore, another was needed. Using the results from the computer run which generated the data for the determination of the bond stress distribution, an effective area was calculated. The bond stresses were plotted at the different levels of f_s, cover and x; A_e was set equal to $4\pi D^2$. This constant was almost arbitrarily chosen because of the scatter in the bond stresses. At this point, this constant will be used in a prediction equation, but it may be refined after checking the prediction equation with the recorded data.

Variable

The more accurate approach to the effective area is to assume that it is a function of f_s and x. Using the same data as in the

previous section, the following procedure was used. With f_s constant, the bond stress value at a particular x was recorded at different distances from the steel. When there was less than one percent difference in two adjacent values, the distance from the steel was recorded as a point on the boundary of the effective area. This procedure was continued over the ranges of f_s and x. Because of the model, the area was assumed to be a solid of revolution about the steel axis, which can be defined by a curve in the r-x plane. The next step was to determine a curve which best fits these points and from this determine the effective area.

It should be noted that if A_e is a function of x, it must be integrated with u_x in Equation (1),

$$f_{tx} = N\pi D \int_o^x u_x/A_e \, dx \qquad \text{(1, repeated)}$$

Since A_e is a function of x and also appears in the denominator, a simple function is desired. The curve determined by a polynominal regression for the boundary of the effective area was a quadratic in x. This quadratic expression must be squared before integration, making integration almost impossible. For this reason, a bilinear curve was chosen to express the boundary. The expressions for r are

$$r = 6.5 - 2x \qquad 0 < x \leq 2 \qquad (25)$$

$$r = 2.5 \qquad 2 \leq x \leq L/2 \qquad (25a)$$

This gives the following expressions for A_e :

$$A_e = \pi D^2 (6.5 - 2x)^2/4 \qquad 0 < x \leq 2 \qquad (26)$$

$$A_e = 6.25\, \pi D^2/4 \qquad 2 \leq x \leq L/2 \qquad (26a)$$

where x and D are in inches.

The equations for effective concrete area are independent of steel stress and of x, if x is greater than two inches. This means that there is a transition length of two inches from a crack before the effective area becomes constant. This transition length is probably the length of bond destruction as described by Nilson[9]. The above expressions are only valid for a single bar. If N bars are considered, the area would not be N times A_e, but something less because of overlapping. An expression which would be correct for this overlapping would be very complicated and require the knowledge of the distances between bars, and both side and bottom cover. It is beyond the scope of this investigation to refine the expressions for A_e any further. The values obtained from these equations will in most cases be high.

VI. PREDICTION OF CRACK FORMATION

The objective of this investigation was to develop a prediction equation for crack width and spacing. This chapter will present these equations and also compare them with the recorded experimental data on cracks in reinforced concrete.

Prediction Equation

The basic approach was presented by Watstein and Parsons[2] and appears in Section II, but the basic equations will be repeated for completeness. The concrete stress at any point between cracks, f_{tx}, is defined as

$$f_{tx} = N\pi D \int_0^x u_x/A_e \, dx \qquad (27)$$

The maximum concrete stress occurs at the center ($x = L/2$) and cannot be greater than the concrete tensile capacity (f'_t). So, if in Equation (27), f_{tx} is set equal to f'_t and x equal to L/2, the following equation results

$$f'_t = N\pi D \int_0^{L/2} u_x/A_e \, dx \qquad (28)$$

The unknown in Equation (28) is the upper limit of the integral, L/2, which requires that an explicit expression be found for the integral.

There are two cases to consider in the evaluation of this integral: the first, when A_e is assumed constant, and the second, when A_e is assumed bilinear.

Constant A_e

Assuming A_e is a constant with respect to x allows A_e to be removed from the integral in Equation (27). The bond stress distribution determined in Section IV was

$$u_x = 0.000539(f_s)^{1.36}(x)^{-0.245} \qquad \text{(24, repeated)}$$

Introducing this into Equation (28) gives

$$f'_t = \frac{N\pi D}{A_e}\int_0^{L/2} 0.000539(f_s)^{1.36}(x)^{-0.245}\,dx$$

or reducing

$$f'_t = \frac{0.000539\ \pi\ D\ (f_s)^{1.36}}{A_e\ (0.755)}(L/2)^{0.755}$$

and solving for L,

$$L = 2\left[\frac{1400\ A_e\ f'_t}{N\ \ D(f)^{1.36}}\right]^{1.324} \qquad (29)$$

where A_e is in square inches

f'_t and f_s in ksi

L and D in inches

Equation (29) defines the maximum crack spacing when A_e is constant.

The maximum crack width is defined as the summation of unit slips from x = 0 to x = L, or

$$W = 2\int_0^{L/2} s_x\,dx \qquad \text{(8, repeated)}$$

where $s_x = \dfrac{f_{sx} - n f_{tx}}{E_s}$ (7, repeated)

$$f_{sx} = f_s - \frac{N \pi D}{A_s} \int_o^x u_x \, dx \qquad \text{(2, repeated)}$$

$$f_{tx} = \frac{N \pi D}{A_e} \int_o^x u_x \, dx \qquad \text{(1, repeated)}$$

Using Equations 1, 2, 7 and 24 in Equation 8 gives

$$W = \frac{2}{E_s} \int_o^{L/2} \left[f_s - (4/D + n N \pi D/A_e) (0.000539 f_s^{1.36}) x^{0.755}/0.755 \right] dx \qquad (30)$$

Integrating and reducing the above equation gives

$$W = \frac{2}{E_s} \left[f_s(L/2) - (4/D + n \pi ND/A_e) (0.000407 f_s^{1.36}) (L/2)^{1.755} \right] \qquad (31)$$

where E_s and f_s are in ksi

A_e in square inches

L, D and W in inches

L is defined by Equation (29).

The above equations are for constant effective concrete area.

Variable A_e

The basic approach to this case is the same as with a constant

A_e, except now A_e must be included in the integrand. Beginning with Equation (24) again and

$$A_e = \pi D^2 (6.5 - 2x)^2/4 \qquad 0 \leq x \leq 2 \qquad \text{(26, repeated)}$$

$$A_e = 6.25 \pi D^2/4 \qquad 2 \leq x \leq L/2 \qquad \text{(26a, repeated)}$$

Equation (28) can be written

$$f'_t = \frac{0.002156\ N\ f_s}{D^{1.36}} \left[\int_0^2 \frac{x^{-0.245}}{(6.5 - 2x)^2}\, dx + \int_2^{L/2} \frac{x^{-0.245}}{6.25}\, dx \right] \qquad (32)$$

The first integral is very difficult to integrate explicitly, therefore, it was integrated numerically. The value obtained was considered accurate only for three figures, thus

$$\int_0^2 \frac{x^{-0.245}}{(6.5 - 2x)^2}\, dx = 0.12 \qquad (33)$$

Using this constant and integrating the second integral gives

$$f'_t = \frac{0.002156\ N\ f_s}{4.719 D^{1.36}} \left[4.719(0.12) - 1.688 + (L/2)^{0.755} \right] \qquad (34)$$

which can be solved for L,

$$L = 2 \left[\frac{2189\ D\ f'_t}{N\ f_s^{1.36}} + 1.122 \right]^{1.324} \qquad (35)$$

where f'_t and f_s are in ksi

D and L are in inches.

The crack width is still defined by Equation (8) even with variable A_e. Using Equations (2), (7), and (27) in Equation (8), gives

$$W = \frac{2}{E_s} \int_o^{L/2} \left[f_s - \frac{4}{D} \int_o^x u_x \, dx - n \pi ND \int_o^x \frac{u_x}{A_e} \right] dx \qquad (36)$$

Assuming that x will always be greater than two inches,

$$\int_o^x \frac{u_x}{A_e} dx = \int_o^2 \frac{u_x}{A_e} dx + \int_2^x \frac{u_x}{A_e} dx$$

or with the u_x and A_e evaluated

$$\int_o^x \frac{u_x}{A_e} dx = 0.000539 \, f_s^{1.36} \left[\int_o^2 \frac{x^{-0.245}}{(6.5 - 2x)^2} dx + \int_2^x \frac{x^{-0.245}}{6.25} dx \right]$$

reducing still further, using Equation (33) defining the first integral

$$\int_o^x \frac{u_x}{A_e} dx = 0.000539 \, f_s^{1.36} \left[0.12 + 0.212 \, x^{0.755} - 0.212(2)^{0.755} \right] \qquad (37)$$

Introducing Equation (36) into (37), combining terms and integrating gives

$$W = \frac{2}{E_s}\left[f_s (L/2) - \frac{.001626\, f_s^{1.36}}{D} (L/2)^{1.755} - \frac{0.002156\, f_s^{1.36}}{D} Nn \left(0.12 (L/2) + 0.212 \left((L/2)^{1.755}/1.755 - (2)^{0.755} (L/2) \right) \right) \right]$$

where E_s and f_s are in ksi

D, L and W are in inches.

The above prediction equations were checked against the experimental data recorded in Section III. The results of this comparison and all modifications of the prediction equations are presented in the next section.

Comparison of Equations With Data

To determine the reliability of the above prediction equations, comparison was made with the recorded crack width and spacing data reviewed in Section II. Using Equations 29 and 31 with constant effective area, the comparison was not good. Correlation coefficients were 0.40 for crack spacing and 0.20 for crack width. These correlations are much too low to assure reliability of any prediction equation. This points up the error of assuming A_e constant when using the approach of Watstein and Parson's[2]. Some improvement was obtained when the variable effective area was used. Equations 35 and 38 were compared and gave correlation coefficients of 0.55 for L and 0.30 for W which were also too low.

To improve the fit, numerical constants in the prediction equations were rounded off to two significant figures and L was assumed to be the value of maximum crack spacing at f_s = 35 ksi. Since L is the maximum possible crack spacing, it seems logical that beyond some level of steel stress, L does not vary. This can be seen in the experimental data of many investigators. Most researchers agree that when f_s exceeds 30 to 35 ksi, the crack spacing is constant. Equation 35 does not reflect this, so it was assumed that when $f_s >$ 35 ksi, L is constant. Using this new crack spacing in Equation 38 gives better results but is still not satisfactory.

One more step was taken to improve the goodness of fit. Since L had been defined by Equation 20a from the statistical analysis, it was used in Equation 38. Again, this improved the fit, raising the correlation coefficient to 0.54, which was still too low for good prediction equations. No further improvements could be made without disregarding the equations defining bond distribution, effective area and unit slip.

The correlation coefficients of the crack spacing equations were always better than for crack width. This was because there is less error involved in those equations and also because L is used in the crack width equation. A close look must be taken at the basic equations as well as the quantities evaluated by this investigation.

The basic equations neglect the effects of interior cracking, initial stresses and strain and strain concentrations around the steel deformations. The last effect would almost be impossible to include in the equations. The interior cracking is just about as difficult

to include. If interior cracking occurs between exterior cracks, then any equation which simply sums the unit slips will over estimate exterior crack widths. This was observed in both sets of prediction equations. The existance of interior cracks has been shown experimentally by Broms[7] by injecting resin into a cracked specimen. Some means of evaluating interior cracking must be determined before this type of approach will yield good correlations with existing data. Initial stresses and strains can be accounted for by initial values on the steel and concrete. The problem is defining these initial values from experimental investigations.

VII. GENERAL DISCUSSION

As was stated earlier, the objective of this dissertation was to obtain prediction equations for both crack spacing and width for reinforced concrete beams. It was believed that with this information design procedures could be developed to help control cracking in modern reinforced concrete structures. There have been two approaches presented, one using a statistical analysis and the other a classical analysis.

The statistical analysis was made using a very complex non-linear regression analysis of recorded crack information. The results were good prediction equations for both crack width and spacing. Since good equations were obtained, this approach can be considered a good one. One problem with this type of procedure is that sometimes erroneous conclusions can be drawn concerning the importance of some parameters. This can occur when an insignificant parameter happens to have values which are of the same order of magnitude as a dependant variable. For example, in the statistical analysis of crack width, f_y was used as an independant parameter in addition to the others mentioned earlier. It seems obvious that f_y has little or no effect on crack width, but the statistical analysis indicated that it was more important than f_s. When f_y was removed from the independant parameters, a better fit was obtained. Therefore, some knowledge of the importance of the independant parameters considered must be a prerequisite. A good indication of a poor parameter is the improvement in fit when it is removed.

Another problem is the loss of structural reality by neglecting all structural mechanics and going directly to the end product. There are only two places where a knowledge of structural mechanics is needed. The first place is deciding what independant parameters to use and the other is in evaluating the final equation.

The prediction equations obtained from this investigation are better than any other recorded in the literature. Gergely and Lutz's [10] equation for crack width was correlated with the same data and had a correlation coefficient of 0.895 compared with 0.981 from this study. Their expression requires pre-calculation of a number of constants while Equation 20 does not. Both equations have the same limitations because the same data was used to determine each equation.

The classical approach here refers to the basic approach used by Watstein and Parsons[2] to analyze cracking reinforced concrete. Beginning with the basic equations of Watstein and Parsons and defining the bond stress distribution and effective concrete area, the prediction equations were determined. The basic equations are simply the equilibrium equations expressed in terms of stress and unit slip.

The experimental program was designed to verify the analytical model, which it did. The concrete strain gage results were not good. The reasons were examined in detail in Section IV. The steel strain gages gave good and consistent results in all but Test 4. The gages in Test 4B gave much lower values than in any other test, and there seems to be no obvious reason for this. The photoelastic results were fair in magnitude and good in pattern. This is all that could realistically be expected considering the error involved in translating

fringe patterns into stress values.

Considering the tests as a whole, there are a few comments which seem necessary. The first concerns the model and how it approximates the actual reinforcing bar in concrete. With only half of the bar covered with concrete, the model is not symmetrical. Strain gages were placed on the steel to determine the magnitude of bending which was found to be small compared to the other strains (less than 5%). The deformations on the bar probably caused more bending than the non-symmetry of the model. Slight bending was even present in the steel stress-strain relationship test, when no concrete was present. The deformations on the steel are not symmetric and, may have introduced this bending because they did not seat properly in the jaws of the testing machine.

The photoelastic results could have been improved if another polariscope had been available. If only one reading is taken with the circular polariscope, only shearing stresses can be obtained. However, if two readings are taken at the same load but at different angles, all principle stresses could be determined. This means that the polariscope must be moved at each load level or that the loading must be repeated so that the second readings could be made. The first alternative requires a great deal of moving and resetting during the test which is not a good procedure to use when testing concrete because of creep. The second alternative is not good practice when measuring bond transfer. As reported by Bresler and Bertero[5], the bond transfer deteriorates with repeated loading. To assure good results, there should be two polariscopes or a polariscope with two

light sources.

The analytical model used was a finite element representation of the axially reinforced concrete cylinder in tension. The material properties of the concrete and steel were the usual values except that the concrete was described in tension as bilinear. Little experimental data exist which define the stress-strain curve of concrete in tension, therefore, some property values were assumed by evaluating the experimental results. The bond element was a rubber-like ring around the steel, with its material properties determined by matching experimental results with analytical results. A great deal of research is needed in this area of bond transfer between concrete and steel in order to define the material properties more precisely.

The finite element approach seems to be the most promising new analytical tool developed recently. This approach allows the consideration of the non-homogeneity and non-linearity of concrete. Bond transfer can be considered, if certain constants can be evaluated by experimental research. Cracks can be considered by inputting cracks where concrete stresses are greater than its tensile capacity. This particular use of finite elements in reinforced concrete must presently be restricted to research, but the effects of its use in research will be seen in design criteria in the near future.

The poor prediction equations developed by the classical method indicate the difficulty of defining the bond distribution and effective concrete area. Both of these quantities influence the crack formation a great deal and, therefore, precise expressions must be obtained for each. This investigation could not determine these quantities

accurately. Another consideration which has been overlooked is interior cracking. The crack width was defined as the sum of the unit slips between two adjacent cracks regardless of the number of interior cracks present. Broms[7] indicated experimentally that many interior cracks do form next to the steel and, therefore, exterior cracks will be of smaller magnitude than predicted. The prediction equation defined by the classical method gave, in almost all cases, higher values than those measured in experimental investigations.

Another problem with the classical approach is the accumulation of "round-off" errors. At many steps, simplifying assumptions were made thus "rounding-off" the theory. These assumptions are often interrelated and, therefore, their errors become confounded in subsequent mathematical operations. Considering these difficulties in expressing the cracking phenomena accurately, the statistical method seems quite superior at the present time.

The application of this investigation to design problems is an important area which needs discussion. Prediction equations have been presented for crack width and spacing which give better correlations thany any other equations available. They could be used in design, if proper safety factors are applied. It is beyond the scope of this dissertation to determine these factors of safety.

Another application of these equations is in further research into the cracking phenomenon. Since crack spacing can be predicted, test beams could be scored at a spacing equal to the predicted crack spacing. This would just about guarantee that the cracks will form at the scores. If this happens, more accurate measurements could be

made of crack width. This procedure could also be used in design cases where cracks cannot be tolerated for asethic reasons. Each score could be filled with a substance of the right color which had high elongation properties. The cracks will form, but will not be seen because of the filler.

VIII. CONCLUSIONS

The following conclusions are made as a result of this investigation:

1. The maximum crack width at the level of the steel in a beam with constant moment section can be predicted very well by the following expression (Eqn 20):

$$W = 0.000012\,(f_s)^{1.29}\,(h)^{-0.036}\,(D)^{0.183}\,(b)^{0.883}\,(COVER)^{0.738}\,(f'_c)^{0.037}\,(N)^{-0.182}$$

2. Average crack spacing in a beam with constant moment section can be predicted quite well using the following expression (Eqn 20a):

$$L_a = 7.84\,(f_s)^{-0.560}\,(h)^{0.443}\,(N)^{-0.835}\,(D)^{-0.612}\,(f'_c)^{-0.099}\,(b)^{0.488}\,(COVER)^{0.064}$$

3. From observation of Equation 20, crack width can be reduced by increasing the number of bars.
4. A finite element model with special bond transfer elements can serve as a great help to researchers in reinforced concrete.
5. The rubber-like ring bond element approximates quite well the bond transfer between steel and concrete.

6. Most bond transfer occurs at the deformation on modern reinforcing bars causing quite pronounced strain concentrations as shown in the photoelastic results.
7. Microcracking and interior cracking influence exterior crack widths a great deal.
8. The randomness of concrete and its cracking make a standard structural mechanics approach seem in error, because it cannot predict crack formation accurately.
9. The best approach to the development of prediction equations for crack formation is a pure statistical analysis.
10. The non-linear regression analysis performed on crack data results in a better prediction equation than any other method available today.

IX. REFERENCES

1. Reis, E. E. Jr.; Mozer, J. D.; Bianchini, A. C. and Kesler, C. E., "Causes and Control of Cracking in Concrete Reinforced with High-Strength Steel Bars—A Review of Research", Engineering Experimental Stat. Bulletin 479 - University of Illinois, August, 1965, p. 61.

2. Watstein, D. and Parsons, D. E., "Width and Spacing of Tensile Cracks in Axially Reinforced Concrete Cylinders," U. S. National Bureau of Standards - Journal of Research, Vol. 31, July, 1943, pp. 1-24.

3. Reis, E. E. and Boresi, A. P., "Stress Distribution in the Cracked Portion of a Reinforced Concrete Beam," Dept. of Theoretical and Applied Mechanics Report No. 250, Univ. of Ill., Aug., 1963.

4. Hognestad, E., "High Strength Bars as Concrete Reinforcement, Part 2. Control of Flexural Cracking," Journal of the PCA Research and Development Laboratories, Vol. 4, No. 1, Jan. 1962, pp. 46-63.

5. Bresler, B. and Bertero, V., "Behavior of Reinforced Concrete Under Repeated Loading," Journal of the Structural Division, Proceedings ASCE, Vol. 94, No. ST6, June 1968, pp. 1567-1592.

6. Wilson, E. L., "Structural Analysis of Axisymmetric Solids," Journal of the A.I.A.A., Vol. 3, 1965, pp. 2269-2274.

7. Broms, B. B., "Crack Width and Crack Spacing in Reinforced Concrete Members," Journal of the ACI, Proceedings Vol. 62, No. 10, October 1965, pp. 1237-1256.

8. Ngo, D. and Scordelis, A. C., "Finite Element Analysis of Reinforced Concrete Beams," Journal of the ACI, Proceedings, Vol. 64, No. 3, March 1967.

9. Nilson, A. H., "Nonlinear Analysis of Reinforced Concrete by the Finite Element Method," Journal of the ACI, Proceedings Vol. 65, No. 9, Sept. 1968, pp. 757-766.

10. Gergely, P. and Lutz, L. A., "Maximum Crack Width in Reinforced Concrete Flexural Members," Causes, Mechanism, and Control of Cracking in Concrete, ACI Publication SP-20, July, 1968, pp. 87-117.

11. Clark, A. P., "Cracking in Reinforced Concrete Flexural Members," Journal of the ACI, Proceedings Vol. 52, No. 4, April 1956, pp. 851-862.

12. Chi, M. and Kirstein, A. F., "Flexural Cracks in Reinforced Concrete Beams," Journal of the ACI, Proceedings Vol. 54, No. 10, April 1958, pp. 865-878.

13. Bertero, V. V., "Discussion of Flexural Cracks in Reinforced Concrete Beams, by Chi and Kirstein (April 1958)," Journal of the ACI, Proceedings Vol. 54, Dec. 1958, pp. 1347-1372.

14. Borges, J. F., "Discussion of Flexural Cracks in Reinforced Concrete Beams by Chi and Kirstein (April 1958)," Journal of the ACI, Proceedings Vol. 54, Dec. 1958, pp. 1347-1372.

15. Rusch, H. and Rehm, G., "Notes on Relation Between Crack Spacing and Crack Width in Members Subjected to Bending," RILEM-Symposium on Bond and Crack Formation in Reinforced Concrete, Stockholm, Vol. II (1957), pp. 507-510.

16. Heterick, R. C., "An Algorithm for Structural Design," Ph.D. Dissertation - V.P.I., May 1968.

17. Zienkiewicz, O. C., The Finite Element Method in Structural and Continuum Mechanics, McGraw-Hill, 1967.

APPENDIX A

Notations

The following is a list of all the notations used. Each entry was first defined when introduced in the body of the dissertation.

A_c = Gross concrete area (square inches)

A_e = Effective concrete area in tension (square inches)

A_s = Area of the reinforcing steel (square inches)

a_i = Regression coefficients

b = Width of beam (inches)

$C_1 = \dfrac{1}{4\int_0^{\frac{1}{2}} f(Q)\,dQ}$ Reference (2)

$C_2 = 8C_1 \int_0^{\frac{1}{2}} dQ \int_0^{Q} f(Q)\,dQ$ Reference (2)

COVER = Concrete cover (inches)

D = Diameter of reinforcing bar (inches)

d = Depth of beam (inches)

E_c = Modulus of elasticity of concrete (ksi)

E_s = Modulus of elasticity of steel (ksi)

e = Error of approximation

$f(Q)$ = Function relating u_m and u_x

f = General stress

f_1, f_2 and f_3 = Principal stresses

f'_c = Compressive strength of concrete (ksi)

f'_t = Tensile strength of concrete (ksi)

f_{tx} = Average tensile stress in concrete at distance x (ksi)

f_s = Tensile stress in the reinforcement at a crack (ksi)

f_{so} = Theoretical value of steel stress at first cracking (ksi) (Reference 2)

f_{sx} = Tensile stress in the reinforcement at a distance x (ksi)

f_y = Yield stress of tension steel (ksi)

h = Total depth of beam

K_1 = $2r_1 u_m E_s/f'_t$ (Reference 4)

L = Maximum possible crack spacing (inches)

L_a = Average crack spacing (inches)

L_m = Minimum crack spacing (inches)

N = Number of reinforcing bars

n = Modular ratio E_s/E_c

p = A_s/A_c

p_e = A_s/A_e

Q = x/L

R = Correlation Coefficient

r = Radius of half-cylinder (inches)

r_1 = Factor reflecting bond distribution (Reference 4)

s_x = Slip per unit length between concrete and steel at distance x

u_x = Bond stress at distance x from a crack (ksi)

u_m = Maximum bond stress (ksi)

W = Maximum width of crack at the level of the steel (inches)

W_m = Minimum width of crack at the level of the steel (inches)

X = Independant parameters

x = Distance from a crack measured along the reinforcing bar (inches)

Y = Dependant variable

ϵ_s = Strain in the steel at a crack

ϵ_{sx} = Strain in the steel at distance x

ϵ = General strain

ϵ_1, ϵ_2 and ϵ_3 = Principal strains

ν = Poisson's ratio

APPENDIX B

Strain Gage Data

The following tables are directly from the tests without corrections. All strain readings are in micro-inches per inch and loads in pounds. The steel stresses recorded were calculated by dividing the load by the nominal area of steel bar. This stress is the stress in the steel outside the concrete.

The gages are numbered for easy reference in Figures 9, 10, and 11. The gage numbers shown in the first six tables refer to Figures 10 and 11. The last two tables from Test 4 refer to Figure 9.

TABLE III

Concrete Strain Gage Data From Test 1

Load Pounds	Steel Stress (ksi)	Concrete Strain (μ in/in.) Gage 7	Gage 8	Gage 9	Gage 10	Gage 11	Gage 12	Gage 13	Gage 14
Half-Cylinder A									
0	0	0	0	0	0	0	0	0	0
11,250	56.25	- 8	- 5	-47	- 5	-815	- 77	20	3
Half-Cylinder B									
0	0	0	0	0	0	-	-	0	0
2,200	11.0	57	79	75	56	-	-	78	91
3,920	19.6	67	97	92	66	-	-	5	-34
5,980	29.9	27	37	42	28	-	-	-17	-30
7,880	39.4	1	0	10	15	-	-	-27	-30
9,800	49.0	-15	-17	- 7	- 7	-	-	-30	-30
12,280	61.4	-30	-38	-33	-19	-	-	-21	-15

TABLE IV

Concrete Strain Gage Data From Test 2

Load Pounds	Steel Stress (ksi)	Concrete Strain (μ in/ in.)							
		Gage 7	Gage 8	Gage 9	Gage 10	Gage 11	Gage 12	Gage 13	Gage 14
Half-Cylinder A									
0	0	0	0	0	0	0	0	0	0
5,200	6.58	33	43	48	22	- 80	-38	5	0
9,850	12.47	55	109	128	37	-112	-58	11	7
14,850	18.80	71	227	209	55	-109	-71	25	20
19,750	25.00	73	340	238	59	-107	-91	23	34
24,800	31.39	4,833	5,493	4,850	27	- 59	-50	18	31
29,200	36.96	8,660	9,583	8,557	115	- 45	-45	17	38
35,750	45.25	a	19,523	a	315	- 52	-51	8	0
Half-Cylinder B									
0	0	0	0	0	0	-	-	0	0
5,600	7.09	45	86	74	60	-	-	66	45
10,150	12.85	53	97	97	81	-	-	156	103
14,700	18.61	43	75	88	80	-	-	120	91
19,500	24.68	29	75	83	67	-	-	279	21
24,400	30.89	17	69	69	47	-	-	252	0
29,300	37.09	2	47	58	7	-	-	249	-7
34,600	43.80	-7	35	55	-28	-	-	239	-1

a - Gage Fractured

TABLE V

Concrete Strain Gage Data From Test 3

Load Pounds	Steel Stress (ksi)	Concrete Strain (μ in/in.)							
		Gage 7	Gage 8	Gage 9	Gage 10	Gage 11	Gage 12	Gage 13	Gage 14
Half-Cylinder A									
0	0	0	0	0	0	0	0	0	0
15,000	9.62	20	87	89	35	- 5	10	60	95
29,800	19.10	- 4	80	110	33	- 7	17	125	212
44,400	28.46	- 7	75	99	20	- 6	19	213	261
59,400	38.08	- 6	79	88	27	0	22	365	285
73,600	47.18	-10	65	65	35	- 1	24	534	258
79,600	51.03	-10	63	48	34	- 1	23	636	250
Half-Cylinder B									
0	0	0	0	0	0	-	-	0	0
16,100	10.32	30	45	0	39	-	-	105	7
29,600	18.97	42	63	- 36	49	-	-	293	10
43,800	28.08	37	59	-112	6	-	-	1,180	- 21
58,500	37.50	- 4	23	-138	- 9	-	-	5,419	- 7
70,500	45.19	14	40	-101	- 7	-	-	8,440	40
80,300	51.47	10	38	- 90	14	-	-	10,055	119

TABLE VI

Steel Strain Gage Data From Test 1

Load Pounds	Steel Stress (ksi)	Steel Strain (μ in/in.)					
		Gage 1	Gage 2	Gage 3	Gage 4	Gage 5	Gage 6
Half-Cylinder A							
0	0	0	0	0	0	0	0
11,250	56.25	3,546	1,824	2,408	1,942	2,117	2,436
Half-Cylinder B							
0	0	0	0	0	0	-	0
2,200	11.0	251	235	519	260	-	408
3,920	19.6	537	490	820	567	-	720
5,980	29.9	986	1,032	1,136	1,173	-	1,064
7,880	39.4	1,323	1,496	1,376	1,657	-	1,350
9,800	49.0	1,671	1,973	1,613	2,115	-	1,676
12,280	61.4	2,137	2,536	1,710	2,713	-	2,208

TABLE VII

Steel Strain Gage Data From Test 2

Load Pounds	Steel Stress (ksi)	Steel Strain (μ in/in.)					
		Gage 1	Gage 2	Gage 3	Gage 4	Gage 5	Gage 6
Half-Cylinder A							
0	0	0	0	0	0	0	0
5,200	6.58	186	163	58	161	142	125
9,850	12.47	375	340	270	350	362	361
14,850	18.80	583	555	516	564	591	593
19,750	25.00	786	780	785	794	858	896
24,800	31.39	1,013	1,142	1,070	1,161	1,155	1,223
29,200	36.96	1,175	1,392	1,265	1,403	1,352	1,474
35,750	45.25	1,466	1,745	1,645	1,743	1,656	1,845
Half-Cylinder B							
0	0	0	0	0	0	-	0
5,600	7.09	168	228	243	239	-	282
10,150	12.85	327	446	379	468	-	447
14,700	18.61	507	680	570	686	-	620
19,500	24.68	696	910	742	915	-	791
24,400	30.89	893	1,147	903	1,155	-	980
29,300	37.09	1,095	1,398	1,184	1,408	-	1,194
34,600	43.80	1,324	1,681	1,590	1,700	-	1,561

TABLE VIII

Steel Strain Gage Data From Test 3

Load Pounds	Steel Stress (ksi)	Steet Strain (μ in/in.)					
		Gage 1	Gage 2	Gage 3	Gage 4	Gage 5	Gage 6
Half-Cylinder A							
0	0	0	0	0	0	0	0
15,000	9.62	335	357	301	374	392	410
29,800	19.10	675	675	590	692	705	725
44,400	28.46	1,050	965	881	991	1,007	1,040
59,400	38.08	1,395	1,265	1,210	1,310	1,330	1,384
73,600	47.18	1,678	1,635	1,608	1,689	1,706	1,790
79,600	51.03	1,798	1,785	1,764	1,845	1,856	1,960
Half-Cylinder B							
0	0	0	0	0	0	-	0
16,100	10.32	235	475	555	477	-	470
29,600	18.97	516	789	879	786	-	769
43,800	28.08	830	1,078	1,135	1,087	-	1,082
58,500	37.50	1,213	1,329	1,326	1,357	-	1,382
70,500	45.19	1,545	1,540	1,510	1,582	-	1,624
80,300	51.47	1,790	1,740	1,745	1,781	-	1,825

TABLE IX

Steel Strain Gage Data Test 4A

Load Pounds	Steel Stress (ksi)	Steel Strain (μ in/in.) Gage 1	Gage 2	Gage 3 Gage 4	Gage 5 Gage 6	Gage 7 Gage 8	Gage 9 Gage 10	Gage 11 Gage 12
0	0	0	0	0	0	0	0	0
				0	0	0	0	0
5,750	7.28	191	244	230	285	173	225	183
				230	221	66	29	97
10,200	12.91	358	457	418	485	253	323	257
				418	389	107	56	153
0	0	10	10	10	35	- 8	- 8	- 8
				0	8	- 8	-10	- 8
5,400	6.84	195	255	223	267	125	160	125
				223	205	50	18	83
10,150	12.85	365	470	426	481	264	338	268
				426	376	120	71	160
14,850	18.80	510	633	582	668	344	435	314
				582	538	155	73	185
19,950	25.25	730	848	778	895	458	552	426
				790	705	174	75	240
24,100	30.51	840	960	890	1,040	512	638	493
				914	824	173	88	280
29,000	36.71	1,260	976	950	1,213	625	786	605
				989	947	196	108	345
35,350	44.75	1,484	1,154	1,133	1,483	748	954	754
				1,165	1,108	217	122	375

TABLE X

Steel Strain Gage Data Test 4B

Load Pounds	Steel Stress (ksi)	Steel Strain (μ in/in.) Gage 1	Gage 2	Gage 3 Gage 4	Gage 5 Gage 6	Gage 7 Gage 8	Gage 9 Gage 10	Gage 11 Gage 12
0	0	0	0	0	0	0	0	0
				0	0	0	0	0
5,850	7.41	265	68	84	91	117	105	120
				39	19	-43	-80	-40
10,800	13.67	385	158	165	162	218	217	214
				123	114	95	68	26
300	.38	18	-63	-55	-42	-40	-40	-51
				-74	-58	-78	-91	-52
5,700	7.22	243	41	54	62	85	71	84
				12	6	-40	-84	-46
10,900	13.80	395	151	156	158	210	204	208
				120	112	95	65	29
15,400	19.49	502	238	235	220	304	287	273
				200	200	213	207	77
20,100	25.44	608	312	300	270	370	350	355
				270	290	345	387	149
24,350	30.82	710	406	380	334	435	405	374
				370	407	490	571	193
29,800	37.72	835	483	451	393	505	472	453
				475	531	664	749	306
36,100	45.70	951	560	520	465	593	568	534
				563	630	733	780	297

The vita has been removed from the scanned document

THEORETICAL AND EXPERIMENTAL ANALYSIS OF CRACK FORMATION IN REINFORCED CONCRETE

by

Kenneth Harold Murray

ABSTRACT

With the introduction and use of high strength materials, especially reinforcing steel, cracking and its control have become more important to the designer of modern reinforced concrete structures. Due to the properties inherent in concrete, cracks cannot be eliminated under normal working loads and, thus, the control of cracking must be studied and understood completely. However, it is a complex problem involving a great many parameters and, hence, conclusions regarding the significance of these parameters are difficult to obtain. In this study, three approaches to the analysis of crack formation are presented: experimental, analytical, and statistical.

The experimental model, the axially reinforced concrete cylinder in tension, is used to study the effect of bond distribution on crack width and spacing. This model has been used by many researchers, both in this country and in Europe. Results are presented from half-cylinders in tension instrumented with strain gages and photoelastic material. The strain gages measured concrete and steel strains, and the photoelastic material measured maximum shearing strains in the concrete.

The analytical model is a finite element representation of the axially reinforced concrete cylinder in tension. Material properties used in the analytical model were determined by comparing the results of the experimental tests with the analytical results. The non-linear characteristics of concrete are considered in this model. The results of the analytical model are evaluated to determine a prediction equation for crack width and spacing. These equations are compared with a large volume of data from beam tests recorded in the literature.

The statistical approach uses the same data to determine the important physical parameters in crack formation. A prediction equation is developed using a non-linear regression analysis.

Prediction equations are presented for both crack width and spacing which have good correlation with recorded data. Conclusions are drawn concerning the use of finite elements in reinforced concrete research.